NASA Contractor Report 145226

A Second-Order Closure Analysis of Turbulent Diffusion Flames

A.K. Varma, E.S. Fishburne,
R.A. Beddini

Contract NAS1-12412
June 1977

National Aeronautics and Space Administration
Langley Research Center
Hampton, Virginia 23665

A SECOND ORDER CLOSURE ANALYSIS OF TURBULENT DIFFUSION FLAMES

By Ashok K. Varma, E. Stokes Fishburne, and Robert A. Beddini

Aeronautical Research Associates of Princeton, Inc.

SUMMARY

A complete second-order closure program for the investigation of compressible, turbulent, reacting shear layers has been developed. The equations for the means and the second-order correlations are derived from the time-averaged Navier-Stokes equations. The equations contain third-order and higher-order correlations, which have to be modeled in terms of the lower-order correlations to close the system of equations. The fluid mechanical turbulence models and parameters are the same ones used in previous studies of a variety of incompressible and compressible shear flows. A number of additional scalar correlations have to be modeled for chemically reacting flows, and a "typical eddy" model has been developed for the joint probability density function for all the scalars. A simpler model in which the higher-order scalar correlations are set zero is also being used. The program is capable of handling multi-species, multi-step chemical reactions.

Computations have been carried out using the second-order closure reacting shear layer (RSL) program to study nonreacting and reacting flows. The calculations for a hydrogen-air diffusion flame demonstrate the importance of the inclusion of the concentration fluctuation correlations in the chemical source terms. The neglect of the correlations leads to the prediction of a very thin reaction zone; whereas, when the unmixedness effects are included in the analysis, the correct turbulent flame structure is calculated.

The concept of the "typical eddy" model has been verified for low heat release reacting flows, and substantial progress has been made towards the construction of a complete model including the density correlations.

INTRODUCTION

Predicting the characteristics of turbulent flames (both diffusion flames and premixed flames) is a problem of major importance in many fields of engineering and has been studied off

and on for almost half a century. The problem basically remains unsolved, though a considerable amount of engineering progress has been achieved by experimentation and empiricism. However, a truly predictive solution of the turbulent reacting flow problems has not yet been achieved. Actually, even the simpler problem of predicting turbulent nonreacting flows has not been solved, though considerable advances have been made in recent years in the development of higher-order closure models. The use of these new closure models for nonreacting flows have demonstrated improved predictive capability compared to the eddy viscosity or first-order closure models. A.R.A.P. has been one of the active groups in the development of multi-equation, complete second-order closure modeling of turbulent flows. The application of these higher-order closure procedures to turbulent reacting flows is a reasonable extension of current technology. This report describes the recent advances made at A.R.A.P. on the methodology for the study of chemical reactions in turbulent media.

Turbulent flows involving chemical reactions occur in many situations including industrial and home furnaces, chemical process plants, various propulsive devices such as jet engines, rocket motor-ram jets, chemical and gas dynamic lasers, and exhaust plumes and wakes of reentry vehicles. In effect, almost every practical flow system involving chemical reactions involves turbulent flowfields. The interaction between the chemistry and the turbulence is of significant importance in many of these systems. The interaction is of importance in determining combustion efficiency and pollutant formation as well as many other combustion characteristics, such as ignition and extinction behavior, flammability limits, combustion stability, combustion noise, etc. The dual and often contradictory objectives of increasing the combustion efficiency and controlling pollutant formation require a more fundamental understanding of the combustion process; and one of the major features that has been ignored in most previous studies is the effect of the turbulent fluctuations of concentrations and temperatures on the chemical reactions.

The main reason this problem has been ignored in the past is due to its complexity. The need for understanding the coupling between turbulence and the chemical processes has been appreciated and acknowledged by the early combustion researchers. However, until very recently the analytical and computational capabilities as well as the diagonistic tools to adequately characterize turbulence in reacting flows were not available. Considerable advances have been made in recent years in these areas and it now appears feasible to develop a rational model for turbulent reacting flows using the second-order closure approach.

In a turbulent diffusion flame, the reaction between initially unmixed reactants (i.e., species α and β) takes place primarily at the edges of the streams of α and β that are twisted together and intertwined as a result of the turbulent mixing process. In this situation, although the time average concentrations of the species α and β at a point in the flow may be quite substantial, the reactants may still not be mixed on the molecular level. The local rate of the chemical reaction is governed by the degree of molecular mixing, and is usually significantly lower than the rate that would be calculated using the time average concentrations of the species at that point. The effect of this molecular unmixedness on the reaction can be incorporated by considering the effect of the species correlations, like $\overline{\alpha'\beta'}$, on the mean chemical source terms. Terms of this kind are calculated in a second-order closure analysis.

A number of efforts are now underway to develop a model of this kind. Donaldson and Hilst (ref. 1) studied low heat release chemical reactions and demonstrated the importance of keeping track of the species correlations. An explicit closure model for third-order species correlations was developed, but this is only valid for isothermal flows. Spalding (ref. 2) formulated an eddy break-up model to study the effect of turbulence on the overall combustion process, but the model is only valid for large turbulence Reynolds numbers and ignores the chemical kinetics effects. The major new problem in the analysis of turbulent reacting flows is the modeling of the higher-order scalar correlations that arise from the chemical kinetic source terms. There seems to be a general acceptance that the desirable procedure is to model or calculate the probability density function (pdf) for the scalars. This procedure has been adopted by A.R.A.P., as well as by Rhodes et al. (ref. 3), Bray and Moss (ref. 4), Libby (ref. 5), Lockwood et al. (ref. 6), Borghi (ref. 7), and Spalding (ref. 8).

Most of these approaches still need to make many simplifying assumptions to make the problem tractable. Bray and Libby use the fast chemistry assumption and deal only with a one-dimensional pdf. The approach of Borghi is very similar to ours for the case of a one-step kinetic reaction. However, he also replaces the joint pdf of species and temperature by a one-dimensional pdf which is a very restrictive assumption. The one-dimensional pdf being popularly used in most of these studies is a clipped Gaussian with delta functions at the two edges. Spalding has recently proposed a Lagrangian theory of turbulent combustion which incorporates the kinetic effects of multi-step chemistry and involves calculating the pdf at various points by following the history of various eddies.

The A.R.A.P. approach models the joint pdf of all the scalars in turbulent reacting flows. A procedure has been developed for constructing the pdf using the available information in a second-

order closure analysis. The model is called the "typical eddy" model and involves representing the pdf by a set of delta functions of variable strengths and positions in the scalar phase space. The strengths and positions of these delta functions at every point in the flow are determined from the predicted values of the means and second-order correlations at that point. Kewley (ref. 9) has recently used our concept of the "typical eddy" model in a study of turbulence effects in a chemical laser. The RSL program has also been used for an extensive study of turbulence effects on DF chemical laser flowfields which is detailed in Reference 10.

This report describes the models and the A.R.A.P. Reacting Shear Layer (RSL) program code. Results of model and program verification studies and calculations for the hydrogen-air diffusion flame at conditions corresponding to the experiments of Kent and Bilger (ref. 11) are presented. The calculations demonstrate the importance of including the scalar correlations of the species and density in the chemical source terms for finite rate chemistry calculations to avoid significant errors in predicting the structure of turbulent flames.

SYMBOLS

a	turbulence model parameter
A	turbulence model parameter
b	turbulence model parameter
D	diameter
g_{ij}	matrix tensor
h	sensible enthalpy
k	thermal conductivity reaction rate
p	pressure
P_1, P_2, P_3	turbulence model parameters
q^2	turbulence kinetic energy
r	radial coordinate
$r_{1/2}$	half radius of mean velocity profile
r^*	radius for which $q^2 = \frac{1}{4} q^2_{max}$
Re	Reynolds number

s, s_T	turbulence model parameter
T	temperature
u_i or u, v, w	velocity components
V_c	turbulence model parameter
x, X	axial coordinate
y	normal coordinate
α, β, γ	species mass fractions
ϵ_i	cell size in "typical eddy" model
θ	$T - T_{ambient}$
Λ	turbulent macroscale
λ	turbulent microscale
μ, μ^*	molecular viscosity coefficients
ν	kinematic viscosity = μ/ρ
ρ	density

Superscripts

$\bar{}$, $\langle\ \rangle$	denotes time average
$'$	denotes fluctuation about the mean value

SECOND-ORDER CLOSURE MODEL AND PROGRAM DEVELOPMENT

Basic Equations

The general conservation equations for a turbulent, compressible, multi-component reacting flow system are presented in Appendix A. These are the Navier-Stokes equations for overall mass continuity, conservation of momentum and sensible enthalpy and for species continuity. The perfect gas equation of state is used. The following assumptions are used in the derivation of these equations:

1. The gas is a continuum.

2. No body forces are present.

3. Radiant heat transfer is neglected.

4. There are no overall mass sources.

5. Mass diffusion is only due to a concentration gradient. Fick's diffusion law is used. Thermal and pressure diffusion are neglected.

6. Each component of the gas mixture is thermally perfect.

The dependent variables in these equations are decomposed into a mean and a fluctuating part, and equations for the mean quantities $\bar{u}_i$, $\bar{h}$, $\bar{\alpha}$, $\bar{\beta}$, ... and various second-order correlations, such as $\overline{u_i'u_j'}$, $\overline{u_i'h'}$, $\overline{u_i'\alpha'}$, $\overline{\alpha'\beta'}$, etc. are derived. This system of equations is not complete as the equations contain a number of third-order and higher-order correlations that have to be modeled to obtain a closed set of equations. This is the familiar closure problem in the analysis of turbulent flows. A second-order closure approach involves modeling these higher-order correlations in terms of the means and the second-order correlations. The basic task in accomplishing a second-order closure solution of turbulent flows is the development of suitable models that remain invariant with respect to changes in the flow geometry. The general model parameters can then be obtained by experiments on simple, standard flowfields and the model can be used as a predictive tool for new and more complex flow problems.

The following additional simplifying assumptions are used in the present study:

1. The mean flow is steady.

2. The mean pressure is constant in the direction normal to the mean flow.

3. Fluctuations in μ , μ^* , k are related to the temperature fluctuations by the expressions of the form

$$\mu' = \mu_T T' + \sum_\alpha \mu_\alpha \alpha' = \left.\frac{\partial \mu}{\partial T}\right|_{\bar{T}} T' + \sum_\alpha \left.\frac{\partial \mu}{\partial \alpha}\right|_{\bar{\alpha}} \alpha'$$

$$\mu'_{,i} = \mu_T T'_{,i} + \sum_\alpha \mu_\alpha \alpha'_{,i}$$

4. Third-order correlations involving μ , μ^* , k are neglected.

The various models for the higher-order correlations that have been developed are reviewed in the next section.

Second-Order Closure Models - Nonreacting Flows

Considerable advances have been made in recent years in the development of second-order closure models for nonreacting turbulent flows, by many groups of investigators (refs. 12,13,14). Donaldson and his colleagues at A.R.A.P. have been involved in the development of a multi-equation complete second-order closure procedure for turbulent incompressible and compressible flows (refs. 15,16,17). The models are selected in the simplest possible way consistent with tensor invariance and available experimental data. The model must remain invariant with respect to changes in the flow geometry. The invariant modeling is an important feature in the sense that our goal is a model which, although it is semi-empirical, has no varying constants which must be determined for each new flow. The model must be applicable to a wide class of fluid flows.

The models for various classes of terms that appear in the second-order closure equations for nonreacting flows are briefly described in this section. The same identical models and model constants are also used for these terms in problems of reacting flowfields. The models and the philosophy behind them have been previously described in greater detail in a number of reports and publications (refs. 17,18,19). For the sake of completeness of this report, some of this information has also been included here.

Modeling of pressure fluctuation correlations.- The correlations involving pressure fluctuations are among the more difficult terms to model in a second-order closure analysis. The results for compressible free shear layer flows presented in Reference 15 indicated the need for improved modeling of the pressure diffusion correlations. New models for various pressure correlations in compressible flows have been recently developed. The models are obtained by following a consistent procedure beginning with the Poisson equation for the pressure,

$$\frac{\partial^2 p}{\partial x_i^2} = - \frac{\partial}{\partial x_i}\left(\rho \frac{\partial u_i}{\partial t} + \rho u_j \frac{\partial u_i}{\partial x_j} \right)$$

The equation is resolved into its mean and fluctuating parts to obtain an equation for p'. This can be formally integrated to obtain p' and then expressions for various correlations can be written. The integral cannot be solved, but with the use of certain approximations, it can be used to suggest the form of the modeled terms. The procedure is described in Reference 20. The models are incorporated in the program code but currently are not being used in the computations in the form given below, as parts of the model have not yet been completely tested. Many combustion problems involve relatively low speed flows, and the program is applicable to the study of these systems. However, the extension of the program to high Mach number flows requires the validation of the constants to be used with portions of the pressure models given below.

The pressure fluctuation correlations arise from the pressure gradient terms in the momentum and energy equations (Eqs. A-3 and A-4)*. The term is typically of the form $\overline{\phi' p'_{,k}}$.

$$\overline{\phi' p'_{,k}} = (\overline{p'\phi'})_{,k} - \overline{p'\phi'_{,k}} \quad .$$

Models have been developed for the two terms on the right-hand side. The terms appear in many of the second-order closure equations. For example, $\overline{p'u'_j}$ and $\overline{p'u'_{j,k}}$ appear in the equations for $\overline{u'_j u'_k}$ (Eq. A-16) and $\overline{u'_j h'}$ (Eq. A-18). Similarly $\overline{p'h'}$ and $\overline{p'h'_{,j}}$ appear in the equations for $\overline{u'_j h'}$ and $\overline{h'h'}$ (Eq. A-17).

Pressure diffusion terms

$$\overline{p'u'_i} = P_1 \bar{\rho} \Lambda^2 \frac{\partial \bar{u}_m}{\partial x_n} \left[\frac{1}{2} (\overline{u'^n u'_i})_{,m} - \frac{1}{4} \left\{ \delta^n_m (\overline{u'_i u'^p})_{,p} + g_{mi} (\overline{u'^n u'^p})_{,p} \right\} \right.$$

$$\left. + \frac{1}{2} \left\{ \delta^n_m \, \overline{u'_i u'^p_{,p}} - g_{mi} \, \overline{u'^n u'^p_{,p}} \right\} \right] + P_2 \bar{\rho} \Lambda q (\overline{u'_i u'^p})_{,p} \qquad (1)$$

$$\overline{p'h'} = P_1 \bar{\rho} \Lambda^2 \frac{\partial \bar{u}_m}{\partial x_n} \left[(\overline{h'u'^n})_{,m} - \frac{1}{3} \delta^n_m (\overline{h'u'^\ell})_{,\ell} \right.$$

$$\left. + \frac{1}{3} \delta^n_m \, \overline{h'u'^\ell_{,\ell}} \right] + P_2 \bar{\rho} \Lambda q (\overline{h'u'^\ell})_{,\ell} \qquad (2)$$

*The A in the Equation numbers refers to Appendix A.

Tendency-towards-isotropy terms

$$\overline{p'u'_{i,j}} = P_3\bar{\rho}\,\frac{\partial u_m}{\partial x_n}\left[g_{mj}\overline{u'^n u'_i} - \frac{1}{3}\,\delta^n_m\,\overline{u'_i u'_j} - \frac{1}{3}\,g_{ij}\,\overline{u'^n u'_m} + \frac{1}{9}\,\delta^n_m\,g_{ij}q^2\right] - \frac{1}{2}\,\frac{\bar{\rho}q}{\Lambda}\left[\overline{u'_i u'_j} - \frac{1}{3}\,g_{ij}q^2\right] \quad (3)$$

$$\overline{p'h'_{,i}} = P_3\bar{\rho}\,\frac{\partial \bar{u}_m}{\partial x_n}\left[\frac{1}{3}\,\delta^n_m\,\overline{u'_i h'} - \frac{1}{2}\,\delta^n_i\,\overline{u'_m h'} - \frac{1}{2}\,g_{mi}\,\overline{u'^n h'}\right] - 0.8\,\frac{\bar{\rho}q}{\Lambda}\,\overline{u'_i h'} \quad (4)$$

In these models, Λ is the turbulent macro-scale length. The major change compared to the models used in References 15 and 18 is the addition of terms involving the mean strain $\partial\bar{u}_m/\partial x_n$. The constant P_2 has been selected to be 0.1 from the studies in Reference 18. The constants P_1 and P_3 associated with the mean strain terms are still under investigation and have to be calibrated using data for compressible shear flows.

Modeling of third-order velocity correlations.-These terms represent the process by which various second-order correlations are transferred from one part of the flow to another without any net production or loss. These terms appear in all the second-order correlation transport equations. For example, $\overline{u'_i u'_j u'_k}$ and $\overline{u'_i u'_j \rho'}$ appear in Eq. A-16, $\overline{u'_i h' h'}$ and $\overline{u'_i \rho' h'}$ are present in Eq. A-17, etc. The most popular modeling of these transport terms is as a gradient diffusion process. A number of different gradient diffusion forms has been proposed (ref. 17). Following previous studies (refs. 15,18), a simple gradient diffusion model is adopted that satisfies the tensor symmetry, and has a scalar diffusion coefficient. The models are of the form:

$$\overline{u'_i u'_j u'_k} = -V_c \Lambda q\left[(\overline{u'_i u'_j})_{,k} + (\overline{u'_j u'_k})_{,i} + (\overline{u'_k u'_i})_{,j}\right] \quad (5)$$

$$\overline{u'_i u'_j \phi'} = -V_c \Lambda q\left[(\overline{u'_i \phi'})_{,j} + (\overline{u'_j \phi'})_{,i}\right] \quad (6)$$

$$\overline{u'_i \phi' \phi'} = -V_c \Lambda q\left[(\overline{\phi' \phi'})_{,i}\right] \quad (7)$$

In Eqs. (6) and (7), ϕ' represents any scalar variable (T', h', c_α', ρ', etc.). V_c was established equal to 0.1 by comparing model results with experimental data in free jets and shear layers. Due to the lack of detailed experimental data in compressible and reacting flows, the same diffusion constant is used as an initial estimate for the velocity diffusion of all correlations.

An alternate set of model constants for pressure and velocity diffusion has been used in atmospheric flow studies. In these studies (refs. 16,17), $P_2 = -0.3$ and $V_c = +0.3$. There are now some indications that this is a somewhat better model on the basis of some recent studies of mixing layer flows of two species, but further work is still continuing to settle this difference.

Dissipation correlations.- The dissipation correlations of the form $g^{mn}(\overline{u'_{j,m}\, u'_{k,n}})$ appear in the equation for $\overline{u'_j u'_k}$ (Eq. A-16) when the viscous terms $\overline{u'_k \tau'_{j,\ell}}$ and $\overline{u'_j \tau'_{k,\ell}}$ are expanded. These terms measure the effect of viscous decay on the second-order correlations. Viscous dissipation is expected to be the major loss mechanism for the turbulence kinetic energy and other correlations. Lewellen et al. (ref. 21) suggest that an isotropic dissipation model is more suitable than the completely anisotropic dissipation model used by Donaldson (ref. 18). However, it is likely that low Reynolds number dissipation will be anisotropic and the following form of the model, which goes to the correct limits for small and large Reynolds numbers is now used.

$$g^{mn}(\overline{u'_{j,m}u'_{k,n}}) = g_{jk}\frac{q^2}{3\lambda^2} + \frac{a}{\Lambda^2}\left(\overline{u'_j u'_k} - g_{jk}\frac{q^2}{3}\right) \tag{8}$$

λ is the Taylor microscale length, and Rotta's form for it is used,

$$\lambda^2 = \frac{\Lambda^2}{a + \frac{bq\Lambda}{\nu}}$$

Detailed studies of the flat plate incompressible boundary layer (ref. 22) have led to a revision in the value of a form 2.5 to 3.25. The constants a and b are:

$$a = 3.25$$

$$b = 0.125$$

Dissipation correlations of the same type appear in all the second-order correlations from the molecular transport terms. The models for all the other dissipation correlations involving scalar fluctuations are of the following form:

$$g^{mn}\,\overline{T'_{,m}T'_{,n}} = s\,\frac{\overline{T'T'}}{\lambda^2} \tag{9}$$

$$s = 1.8$$

$$g^{mn}\,\overline{u'_{i,m}T'_{,n}} = s_T\,\frac{\overline{u'_i T'}}{\lambda^2} \qquad (10)$$

$$s_T = 1.0$$

The models for the dissipation of the other scalars are of the same form as Eqs. (9) and (10).

Turbulent macro-scale Λ.- It is necessary to specify the turbulent scale Λ, used in many of the modeled terms, in order to complete the closure of the second-order correlation equations. For nonreacting flows, both an algebraic specification of the scale based on the gross features of the flowfield, and the use of a modeled dynamic differential equation to calculate the local scale at each point in the flowfield have been used. The latter procedure does lead to somewhat better results, but up to this time it has not been possible to develop a universal model scale equation. Some of the parameters in the scale equation have to be changed for different flow geometries. This problem can be readily appreciated when one realizes that all of the terms in the scale equation have to be modeled. The scale equation contains much more arbitrariness than the other second-order correlation equations.

With the uncertainty involving the use of an incompressible dynamic scale equation and the lack of a scale equation formulation for compressible and/or reacting flows, it was decided to simply use an algebraic specification of the macroscale in the reacting shear layer (RSL) computer code. The scale is determined using either the mean axial velocity, $\bar{u}$, profile or the profile of the turbulence kinetic energy, q^2. For axisymmetric flows,

1. $\Lambda = 0.5\, r_{1/2}$, where $r_{1/2}$ is the half radius of the mean axial velocity $\bar{u}$.
2. $\Lambda = 0.2\, r^*$, where r^* is the radius where $q^2 = \frac{1}{4}\, q^2_{max}$.

The use of the turbulence kinetic energy profile for determining Λ gives better results for nonreacting flows. At the present time there is no clear conclusion as to the preferable scale procedure for reacting flows, due to uncertainties in other modeling approximations. The scale based on the mean axial velocity profile has been used in most of the current reacting flow calculations.

Second-Order Closure Models - Scalar Correlations in Reacting Flows

The major new difficulty in the second-order closure computation of turbulent reacting flows over that for nonreacting flows is the need for modeling of scalar correlations, such as $\overline{k'\alpha'}$, $\overline{k'\alpha'\beta'}$, $\overline{\alpha'\alpha'\beta'}$, etc. that appear in the equations.

The "typical eddy" model for the joint probability density function of all the scalars (ρ , h , T , α_i , k) has been developed by Donaldson and Varma (refs. 23,24) that appears to be very promising for the modeling of all such scalar correlations.

Consider a simple one-step reaction involving two reactant species α and β and one product species γ , i.e., $\alpha + \beta \rightarrow \gamma$. Even for this very simple chemical system, a very large number of higher-order scalar correlations appear in the equations and particularly in the chemical source term. Instead of attempting to individually model all these terms, there is a general acceptance among many of the research groups active in this area, to model or calculate directly the probability density function (pdf) of the scalars. In general, the pdf will be a continuous function in the scalar phase space and attempts have been made to model the pdf by various continuous functions (refs. 4, 6, 7) for the case of one-dimensional pdf's. However, for a multi-dimensional joint scalar pdf it is much more difficult to guess the appropriate shapes for the pdf. The "typical eddy" model proposes to represent the joint pdf by a set of delta functions of variable strengths and positions in the scalar phase space. The sketch illustrates how the important features of a complicated continuous pdf may be represented by a series of delta functions, and also shows an alternate "box" representation for the two-dimensional delta function pdf. Once the joint pdf has been modeled, it is possible to calculate

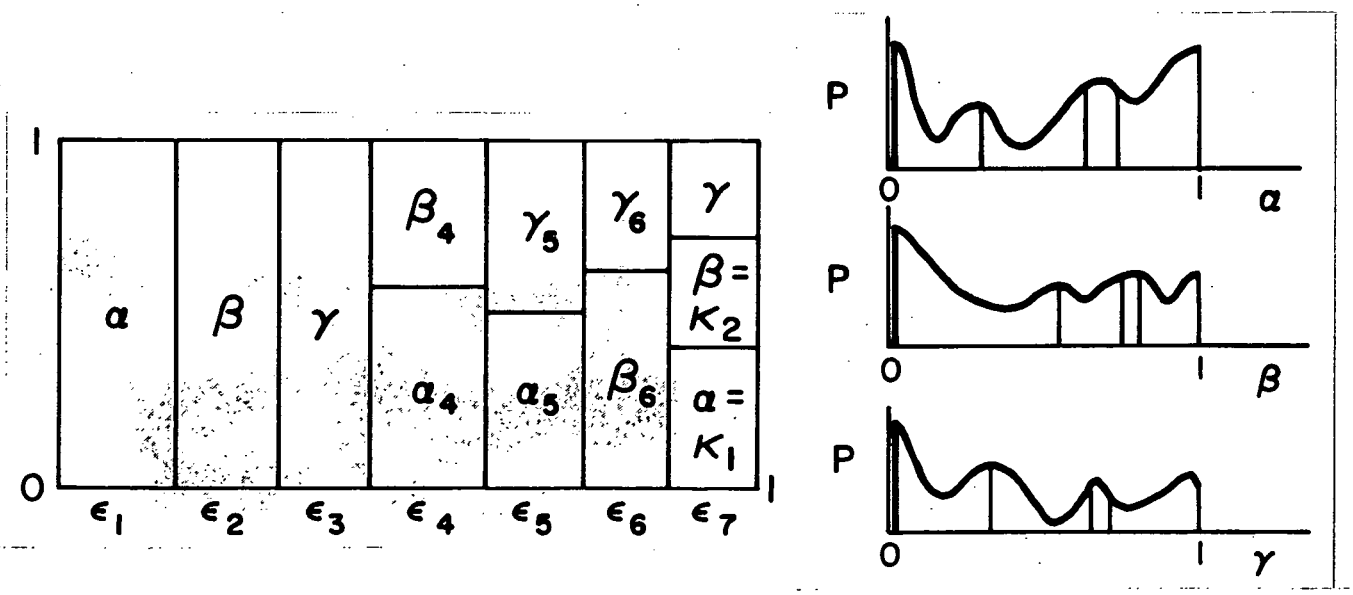

all the required higher-order scalar correlations and to close the set of second-order correlation equations for turbulent reacting flows.

The construction of the "typical eddy" model is an attempt to utilize all the available information from a second-order closure analysis to define the joint pdf of the scalars. The degrees of freedom in the model, i.e., the number of delta functions, their strengths and their location in the phase space, are limited by the number of independent parameters available in a second-order closure calculation. The location of some of the delta functions is decided on physical grounds. The positions of the other delta functions and the strengths of all the delta functions at every point in the flow are determined from the values of the means and second-order correlations obtained from the solution of the transport equations. The method of construction of the delta function pdf model guarantees that the model reproduces the first-order and second-order moments of the flow.

The complete second-order closure program for a three-species flow system provides information on 13 independent first- and second-order correlations - $\bar{\alpha}$, $\bar{\beta}$, $\overline{\alpha'\beta'}$, $\overline{\alpha'\gamma'}$, $\overline{\beta'\gamma'}$ $\overline{\alpha'\rho'}$, $\overline{\beta'\rho'}$, $\overline{\rho'\rho'}$, $\bar{h}$, $\overline{h'h'}$, $\overline{\alpha'h'}$, $\overline{\beta'h'}$, and $\overline{\rho'h'}$; so the complete model can have no more than 13 parameters. Figure 1 shows the model that has been selected after extensive studies. The model has exactly 13 parameters to be determined. The typical eddy is considered to have the following structure. For a fraction ε_1 , the eddy contains only the species α . The cell has a sensible enthalpy h_α and, since for a single species flow from a constant enthalpy source the model must allow enthalpy fluctuations, $\overline{h'h'}$, due to boundary conditions and/or viscous heating, a Δh has been added for half of the cell. For a single species flow, the enthalpy structure has just two parameters (h_α and Δh) to be calculated from the values of $\bar{h}$ and $\overline{h'h'}$ obtained from the transport equations. In the model currently being used in the reacting shear layer programs, the same Δh is used for all the cells. For a fraction ε_2 , the eddy contains only species β with an enthalpy h_β , and for a fraction ε_3 , the eddy has only the pure species γ and has the corresponding enthalpy h_γ . For fractions ε_4 , ε_5 , and ε_6 , the eddy is assumed to contain α and β , α and γ , and β and γ , respectively, in a state of molecular mixedness. There appear to be two equally reasonable choices for the proportions of the species in these cells. One can consider the species to be present in either equal amounts or amounts proportional to their average values at that point in the flow. The current program retains both of these options at the present time, and further test runs will indicate the more desirable model. Corresponding average values are used for the enthalpies of the cells. Finally, an ε_7 fraction of the eddy contains all three species α , β , and γ in a molecular mixture of proportions κ_1 , κ_2 , and $1 - \kappa_1 - \kappa_2$. The enthalpy of cell 7 is h_7 . The model has 13 unknowns (ε_1 through ε_6 , κ_1 , κ_2 , h_α , h_β , h_γ , h_7 ,

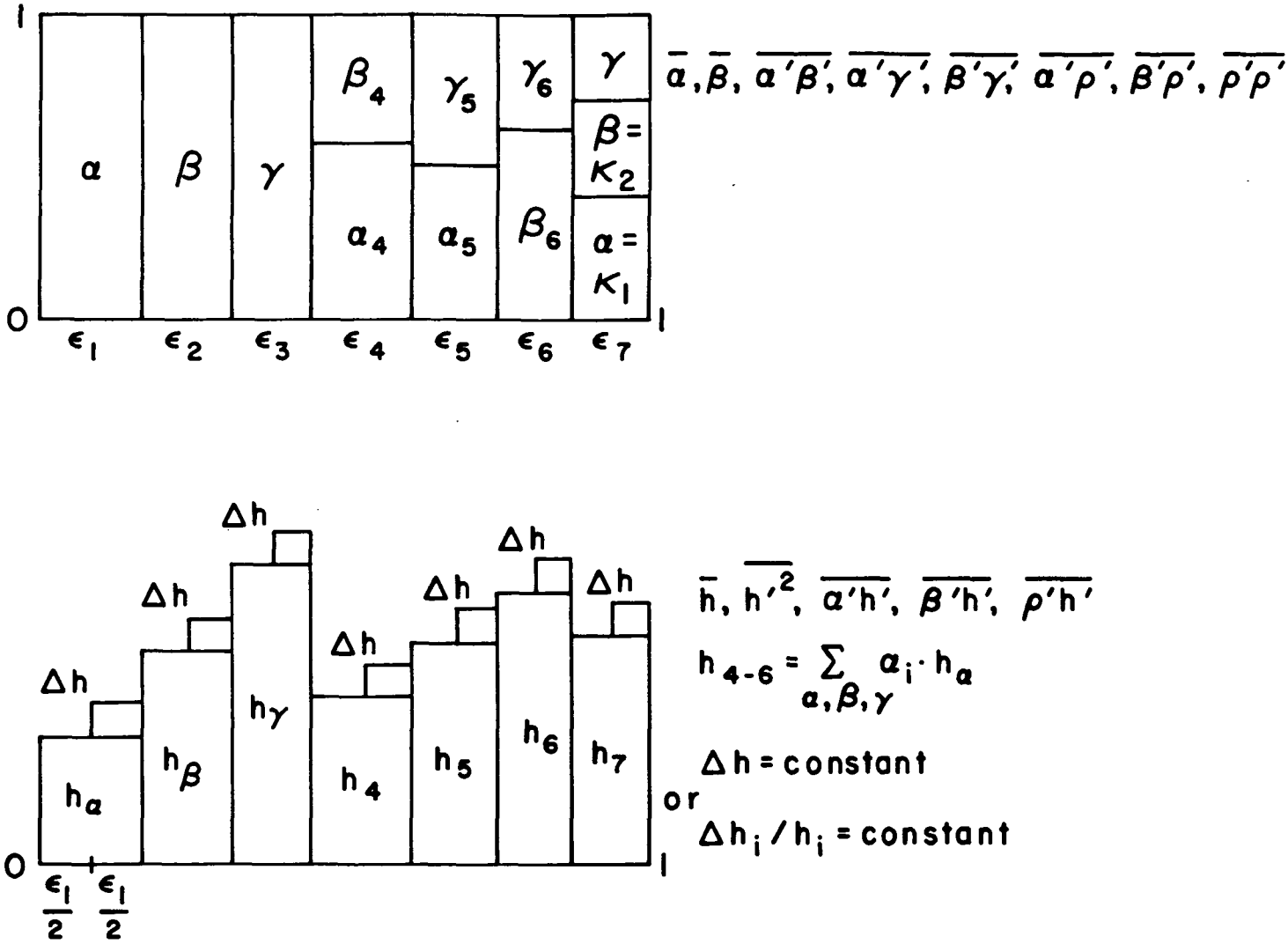

Figure 1. Complete three-species "typical eddy" model.

and Δh) note $\left(\sum_{1-7} \epsilon_i = 1\right)$ to be determined from the 13 available independent correlations by matching the moments of the model to the values predicted by the equations. The procedure for the construction of the "typical eddy" model is described in Appendix D, and further details can be seen in References 23 and 24. The model can be constructed at any desired time from the second-order closure turbulence calculation in progress. Once the species and enthalpy distribution functions have been established, the corresponding distributions for the other scalars - temperature, density, and the reaction rate, k - can be constructed. The complete nonlinear Arrhenius rate expression can be used for constructing the k distribution function; there is no need to expand the exponential term. All scalar correlations required to close the system of second-order correlation equations can now be calcualted from this joint probability density function.

The construction of the complete "typical eddy" model described above requires the solution of a set of nonlinear algebraic equations. The nonlinear equations arise due to the density correlations and a simplified "typical eddy" model was proposed which was easier to implement for the initial testing of the concept of the model.

Simplified "typical eddy" model.- The simplified "typical eddy" model does not consider the density fluctuation correlations in the construction of the model. The neglect of the density correlation results in only nine moments $\bar{\alpha}$, $\bar{\beta}$, $\overline{\alpha'\beta'}$, $\overline{\alpha'\gamma'}$, $\overline{\beta'\gamma'}$, $\bar{h}$, $\overline{h'h'}$, $\overline{\alpha'h'}$, and $\overline{\beta'h'}$ - being available to formulate the model and, therefore, the simplified model can only have nine parameters. The model construction is briefly discussed in Appendix D. Further details of the construction and testing of the simplified "typical eddy" model are described in References 23, 24, and 25. The simplified model results in a linear set of equations for the determination of the cell sizes in the species probability density function, and analytical closed form solutions for the model have been obtained. In contrast, one has had to resort to numerical solutions in the case of the complete three species model, although, some progress has been recently made towards obtaining analytical solutions of the nonlinear equations. This is discussed later in this section.

The simplified model involves the neglect of the density correlations and, therefore, should be valid for flows where density changes are small. The simplified "typical eddy" model has been shown (ref. 26) to be satisfactory for low heat release reacting flows where the density changes could be neglected. However, just how far one could use this simplified scheme could only be tested by actual computations and comparison to experimental measurements. Our studies on chemical laser flows and hydrogen-air flames where significant density changes are involved suggest that the more complete "typical eddy" model has to be used, as was expected, for these flows.

The current reacting shear layer (RSL) computer program is designed to use the simplified "typical eddy" model or an even simpler model designated as the "secondary" model. The model used in a particular test run is conveniently selected as an input option.

Secondary model.- In this model all third-order and higher-order scalar correlations are set to zero. This is designated as the "secondary" model, as distinguished from the primary model which is the "typical eddy" model. Second-order correlations such as $\overline{T'\alpha'}$, $\overline{k'\alpha'}$, and others for which we do not carry transport equations, are now obtained up to second-order accuracy by expansion of explicit thermodynamic relations between the instantaneous variables. When the "typical eddy" model is used, these conversion relations are not necessary as the pdf for ρ,T and k can be constructed directly from the pdf of α_i and h using the thermodynamic relationships. The "secondary" model was initially used during the model development stage but some recent calculations (ref. 26) have indicated that, at least for some simple reacting flows, the two models may predict quite similar results. It can be shown quite easily that the "secondary" model is not correct in a number of limiting cases. For example, in the reaction end limit for a system of three species undergoing the one step reaction $\alpha + \beta \rightarrow \gamma$,

$$\alpha\beta = 0$$

$$\bar{\alpha}\bar{\beta} + \overline{\alpha'\beta'} = 0$$

$$\bar{\alpha}\beta' + \alpha'\bar{\beta} + \alpha'\beta' - \overline{\alpha'\beta'} = 0$$

$$\bar{\alpha}\,\overline{\alpha'\beta'} + \overline{\alpha'\alpha'}\,\bar{\beta} + \overline{\alpha'\alpha'\beta'} = 0$$

$$\overline{\alpha'\alpha'\beta'} = -\bar{\alpha}\,\overline{\alpha'\beta'} - \bar{\beta}\,\overline{\alpha'\alpha'}$$

$$= \bar{\beta}\,\bar{\alpha}^2\left(1 - \frac{\overline{\alpha'\alpha'}}{\alpha^2}\right)$$

$$\neq 0, \text{ in general}$$

Thus, setting the third-order scalar correlations to zero is not a proper model and the good agreement obtained between the results from the "secondary" model and the simplified "typical eddy" model must be simply coincidental. However, it is still an interesting question why the results for some of the flows that we have studied are insensitive to the choice of the model for the higher-order scalar correlations, and work is continuing to explain these observations.

The exothermic reacting flow calculations reported here have been carried out using the "secondary" model. These calculations should be repeated later with the complete "typical eddy" model.

Analytical solution for the complete "typical eddy" model.- Recent studies on chemical laser flows and hydrogen-air diffusion flames have shown that in flows involving large density changes the simplified "typical eddy" model leads to large errors and the more complete model including the density moments has to be used. We have completed the formulation of the nonlinear equations for the complete model and it appears likely that analytical solutions of these nonlinear equations can be obtained. Analytical closed form solutions for a "typical eddy" model for a two species mixing problem have already been obtained. The solution is very promising for it proves that for any statistically consistent set of moments, one can find a rational solution for the model parameters, that is, the strengths of the delta functions are positive and their location is inside the physically realistic region of the scalar phase space. Efforts are underway to obtain similar analytical solutions for the three species model for the reacting flow problems.

The reacting shear layer (RSL) computer program for second-order closure analysis of turbulent reacting flows will be able to incorporate the complete "typical eddy" model with very minor changes.

Multi-Step Chemistry Procedure

The reacting shear layer program and the "typical eddy" model were originally developed for use with three species (α, β, and γ) flowfields, and only permitted the single-step reaction $\alpha + \beta \rightarrow \gamma$. The concept of such an overall reaction may be entirely sufficient in some combustion problems, but for most problems it is necessary to use a set of elementary reaction steps involving many species to correctly describe the system and to obtain results in better agreement with experiments. This conclusion is particularly valid with respect to trace species. Further, the elementary reactions have been studied extensively and the reaction rate parameters are better known. Ideally, one would like to keep track of each species and the correlation between each species and the other species as well as the correlation with certain flow properties. Unfortunately, this desire introduces an enormous number of equations which must be solved in an implicit fashion. The resulting computer time would be prohibitive to the point that the code would simply not be used for engineering calculations. Therefore, a system has been constructed for handling a finite number of species and reactions within the present framework.

To understand the basic philosophy of this reaction scheme, it is useful to consider the expression for the rate of change of a species, α, due to chemistry in a situation in which turbulence may be present. It can be shown that the expression reduces to:

$$\frac{d\bar{\alpha}}{dt} = -\bar{k}\bar{\alpha}\bar{\beta} - [\overline{k\alpha'\beta'} + \overline{\alpha k'\beta'} + \overline{\beta k'\alpha'} + \overline{k'\alpha'\beta'}]$$

Laminar Contribution — Turbulent Contribution

In the absence of turbulence, the rate of change of the species is simply given by the laminar expression. When turbulence is present, all of the other terms must be considered. The computation of these terms, and the other necessary correlations, is the reason the computer time becomes excessive. In the laminar case, such correlations are not required. Thus, the extension of laminar flow situations to hundreds of chemical species and reactions is straightforward since it only requires the addition of another equation for the conservation of mass of each added species. In the turbulent case, the addition of a new species requires the addition of at least three equations for the correlations with the primary flow variables plus an equation for the correlation with each of the other species in the flow. From a practical viewpoint, and the desire to maintain reasonable computation times, it was decided to "track" only three species: α, β, and γ.

In any diffusive reacting flow, one usually has two initially separate streams of fuel (α) and oxidizer (β). These streams are now considered to be known mixtures of a number of chemical species. The streams mix and react following a large number of elementary reactions and form a mixture of product species designated as γ. It is assumed that (1) the composition of mixtures α and β is fixed for the entire flowfield. There are no internal reactions among the species in these two reactant mixtures. (2) All the product species that compose γ are molecularly mixed. There are internal reactions within the γ species mixture. The composition of the mixture γ varies at different points across the flowfield.

Consider the hydrogen-air diffusion flame as an example of the multi-step chemistry procedure. To illustrate the procedure we consider only the two reactions given below. The complete set of reactions that are used in our studies of the hydrogen-air system are presented in Table 1.

$$H_2 + OH \rightleftharpoons H_2O + H$$

$$H_2 + O \rightleftharpoons OH + H$$

Let the α stream be pure hydrogen, $H_2(\alpha)$. The β stream is a mixture of oxygen, $O_2(\beta)$ and nitrogen, $N_2(\beta)$ of known, fixed proportions. The γ product species contains H_2, OH, H, O, O_2, H_2O, N_2, etc. On the basis of the two assumptions mentioned earlier, the interaction between turbulence and ehcmistry only has to be taken into account for reactions between α and β, α and γ, and β and γ. Species within γ are assumed to be molecularly mixed and, therefore, species correlations do not have to be considered for the internal reactions. For convenience, the reaction system given above is rewritten in the following form, tagging each chemical species with the mixture that it is a part of:

$$H_2(\alpha) + OH(\gamma) \xrightarrow{k_{f1}} H_2O(\gamma) + H(\gamma) \qquad \text{one way reaction}$$

$$H_2(\alpha) + O(\gamma) \xrightarrow{k_{f2}} OH(\gamma) + H(\gamma) \qquad \text{one way reaction}$$

$$H_2(\gamma) + OH(\gamma) \underset{k_{r1}}{\overset{k_{f1}}{\rightleftharpoons}} H_2O(\gamma) + H(\gamma)$$

$$H_2(\gamma) + O(\gamma) \underset{k_{r2}}{\overset{k_{f2}}{\rightleftharpoons}} OH(\gamma) + H(\gamma)$$

The chemical source terms for the component species can now be written:

$$\frac{d\overline{H_2(\alpha)}}{dt} = - k_{f1} \left[\overline{H_2(\alpha)}\,\overline{OH(\gamma)} + \overline{H_2'(\alpha)OH'(\gamma)}\right]$$

$$- k_{f2} \left[\overline{H_2(\alpha)}\,\overline{O(\gamma)} + \overline{H_2'(\alpha)O'(\gamma)}\right]$$

$$\frac{d\overline{H_2(\gamma)}}{dt} = - k_{f1}\, \overline{H_2(\gamma)}\,\overline{OH(\gamma)} + k_{r1}\, \overline{H_2O(\gamma)}\,\overline{H(\gamma)}$$

$$- k_{f2}\, \overline{H_2(\gamma)}\,\overline{O(\gamma)} + k_{r2}\, \overline{OH(\gamma)}\,\overline{H(\gamma)}$$

etc.

Transport equations are solved for the second-order correlations $\overline{\alpha'\beta'}$, $\overline{\alpha'\gamma'}$, and $\overline{\beta'\gamma'}$. The additional important assumption is made that quantities like $\overline{H_2'(\alpha)OH'(\gamma)}$ can be simply calculated from these correlations as being proportional to the local mean composition of the mixture.

For example, $$\overline{H_2'(\alpha)OH'(\gamma)} = \frac{\overline{\alpha'\gamma'}}{\left(\frac{\overline{H_2(\alpha)} \cdot \overline{OH(\gamma)}}{\bar{\alpha} \cdot \bar{\gamma}}\right)}$$

The validity of this assumption has to be examined further, but it should not lead to large error. The correct procedure, of course, is to solve separate equations for each such correlation, but this is impractical at the present time.

The above procedure operates within the framework of three overall species mixtures, and all the models and equations developed earlier can be used. The only addition to the program is the solution of mean species conservation equations for all the elemental species.

Numerical Solution of the Equations

The use of the models for various third- and higher-order correlations, as described earlier, in the set of equations for the means and second-order correlations results in a closed set of equations. Equations for the mean variables $\bar{\rho}$, $\bar{u}_i$, $\bar{h}$, $\bar{\alpha}$, and $\bar{\beta}$ and the second-order correlations $\overline{u_i'u_j'}$, $\overline{h'h'}$, $\overline{u_i'h'}$, $\overline{\alpha'\beta'}$, $\overline{\alpha'\gamma'}$, $\overline{\beta'\gamma'}$, $\overline{u_i'\alpha'}$, $\overline{u_i'\beta'}$, $\overline{u_i'\rho'}$, $\overline{h'\alpha'}$, and $\overline{h'\beta'}$ are solved in the present program. The use of the basic shear layer assumptions leads to a set of 23 independent coupled parabolic partial differential equations.

The computer program actually solves a total of 29 equations for a three species system. The additional equations are for $\bar{\gamma}$, $\overline{u'\gamma'}$, $\overline{v'\gamma'}$, $\overline{h'\gamma'}$, $\overline{\alpha'\alpha'}$ and $\overline{\beta'\beta'}$. The redundant equations provide a check on the mass conservation in the program and on the accuracy of the numerical scheme. The numerical integration of the equations is performed by a forward-time, upwind, finite-differencing scheme. The nonlinear terms are handled by quasi-linearization, that is, by evaluating a portion of these terms at the known position, leaving only a linear term containing one of the unknowns. The linearized finite-difference equations are solved in implicit fashion using the general tridiagonal algorithm. However, instead of solving a single large matrix, which would be very time-consuming, the equations are grouped into smaller matrices and the system is solved in 10

separate passes. The equations solved in the various passes are detailed in the table below. The variables are updated only at the end of all the 10 passes. For multi-step chemistry problems, the first pass solves the conservation equations for all the elemental species.

Table RSL Passes

Pass No.	Unknowns
1	$\bar{\alpha}$, $\bar{\beta}$, $\bar{\gamma}$ or $\bar{\alpha}_i$
2	$\bar{u}$, $\langle u'v' \rangle$
3	$\bar{h}$, $\langle v'h' \rangle$, $\langle \rho'v' \rangle$
4	$\langle u'u' \rangle$, $\langle v'v' \rangle$, $\langle w'w' \rangle$
5	$\langle h'h' \rangle$, $\langle u'h' \rangle$, $\langle \rho'u' \rangle$
6	$\langle u'\alpha' \rangle$, $\langle u'\beta' \rangle$, $\langle u'\gamma' \rangle$
7	$\langle v'\alpha' \rangle$, $\langle v'\beta' \rangle$, $\langle v'\gamma' \rangle$
8	$\langle h'\alpha' \rangle$, $\langle h'\beta' \rangle$, $\langle h'\gamma' \rangle$
9	$\langle \alpha'\alpha' \rangle$, $\langle \alpha'\beta' \rangle$, $\langle \alpha'\gamma' \rangle$
10	$\langle \beta'\beta' \rangle$, $\langle \beta'\gamma' \rangle$
+ continuity equation for $\bar{v}$	

The program has the capability of handling both fixed and free shear layer flows for planar and axisymmetric geometries. The initial profiles can be provided using a card or tape input or the program can generate appropriate smooth initial profiles given the properties of the two streams. If the turbulence properties at the initial station are not known, a "spot" of turbulence is input at the initial station to start the turbulent calculations. The turbulence profile is a smooth bell-shaped profile of specified small amplitude and width. It has been shown that the calculated results after approximately 10 diameters downstream are insensitive to the amplitude and width of the initial turbulence profile. The program uses a fourth-order polynomial expression to calculate the temperature dependence of the specific heat of various species. The molecular transport properties μ , μ^* , k , and D are calculated using a power law expression.

Additional details of the program operation for a number of the test runs are discussed later in the report. Appendix C contains a description of the RSL program input deck and the details on the use of the various available options.

MODEL AND PROGRAM VERIFICATION - NONREACTING FLOWS

Introduction

The principal objective of developing a higher-order closure turbulence model than the first-order closure eddy-viscosity models is to obtain a more "universal" model; a model which can be used for analysis of data for a wide class of flowfields with the use of the same invariant set of model constants. Such a model can then be used with a greater degree of confidence for predictive calculations of flow problems for which experimental data are not available or are difficult to obtain. Second-order closure models have shown significant promise of being such a predictive tool.

The fluid mechanical turbulence models being used in the A.R.A.P. second-order closure program have already been extensively tested by comparison of program predictions to experimental data in a variety of basic flow geometries. Previous publications have discussed studies on flat plate boundary layers (refs. 15,22), the planetary boundary layer (ref. 16), and two-dimensional wakes and jets (ref. 26). The two-dimensional reacting shear layer (RSL) code was extended to axisymmetric flows under the NASA contract, and model and program verification studies for axisymmetric jets and wake flowfields and the mixing of two different species in a shear layer geometry have been carried out in the following sample cases.

Axisymmetric Free Jet

The RSL program predictions for an axisymmetric free jet were compared to the experimental measurements of Wygnanski and Fiedler (ref. 27). Detailed measurements of the mean axial velocity profile and the Reynolds stresses were made in the self similar region of the flowfield. The measurements are designated as Test Case 18 in data compiled in the 1972 NASA Free Turbulent Shear Flows Conference (ref. 28).

The A.R.A.P. models have already been tested against this flowfield in previous simpler nonreacting programs (refs. 17,29) and the present repetition of the test case provides a good consistency check for the RSL code. The computations are started using a simple linear (arbitrary) profile for the mean velocity and a triangular distribution for the Reynolds stresses with $\overline{u'u'} = \overline{v'v'} = \overline{w'w'} = 2|\overline{u'v'}|$ at the initial station. The turbulence scale Λ is determined from the turbulence kinetic energy q^2 profile. The model constants for the diffusion terms are $P_2 = -0.3$ and $V_c = +.3$. The constants P_1 and P_3 are set at zero.

Comparisons between RSL program model predictions and experimental data are shown in Figures 2, 3, and 4. Figure 2 compares the mean axial velocity profiles and indicates excellent agreement. Figures 3 and 4 show the results for the normal Reynolds stresses $\overline{u'u'}$ and $\overline{v'v'}$. The predicted values are somewhat low on the centerline. The agreement can be improved for this flow by incorporating the mean strain terms in the pressure correlation models but the values of the corresponding model parameters have not yet been evaluated. Further, to obtain a model that is reasonably good for a wide range of flows, it is best not to fine-tune it to a particular flow. The parameters for the complete pressure models will be selected to improve the model predictions for both incompressible and compressible flows, and then these basic test flows will be reexamined. The RSL program results are consistent with previous A.R.A.P. studies.

Axisymmetric Wake

The second axisymmetric test flow was selected to be the axisymmetric wake measurements of Chevray (ref. 30). A.R.A.P. model predictions have also been compared against other axisymmetric wake measurements in Reference 29. Chevray measured the mean velocity $\bar{u}$ and the Reynolds stress $\overline{u'v'}$ at several axial stations in the wake behind a six-to-one prolate spheroid at a Reynolds number, based on free stream velocity and body length, of 2.75×10^6. The data is NASA Test Case 15 in Reference 28. The measurements at the axial station three diameters downstream of the trailing edge of the body were chosen as the initial conditions for the model calculations. This was assumed to be far enough downstream that our assumption of no axial pressure gradient in the calculations would be valid. The initial conditions for the program run used the measured data for $\bar{u}$ and $\overline{u'v'}$ at $\frac{x}{D} = 3$. The normal stresses at this initial station were not known and were assumed to be $\overline{u'u'} = \overline{v'v'} = \overline{w'w'} = 2|\overline{u'v'}|$. The scale Λ is constant across the flow and is determined from the turbulence energy q^2 profile. The model constants are again $P_2 = -0.3$, $V_c = +0.3$ and $P_1 = P_3 = 0$.

Figure 5 shows the decay of the maximum velocity defect w_D. The model predictions are reasonably good, though the data appears to decay somewhat faster than the analytical predictions. The maximum shear stress $\overline{u'v'}_{max}$ is plotted in Figure 6. The model predicts a higher initial buildup of the shear stress before it begins to decay and is then in good agreement with the data. The predicted profiles of the mean velocity and the shear stress at axial stations $\frac{x}{D} = 9$ and 18 are compared to the measure-

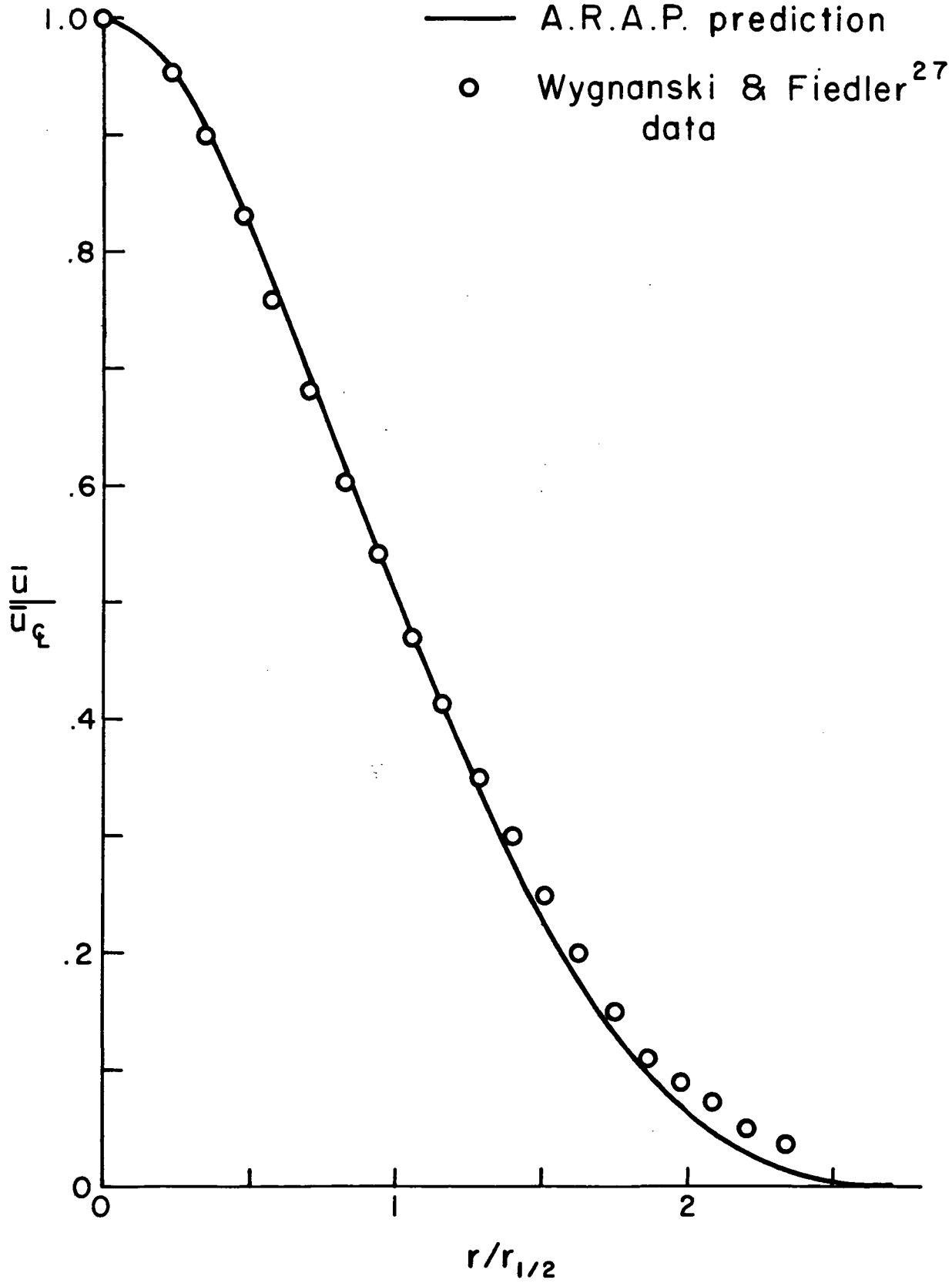

Figure 2. Mean axial velocity profile in a free jet in the self-similar region.

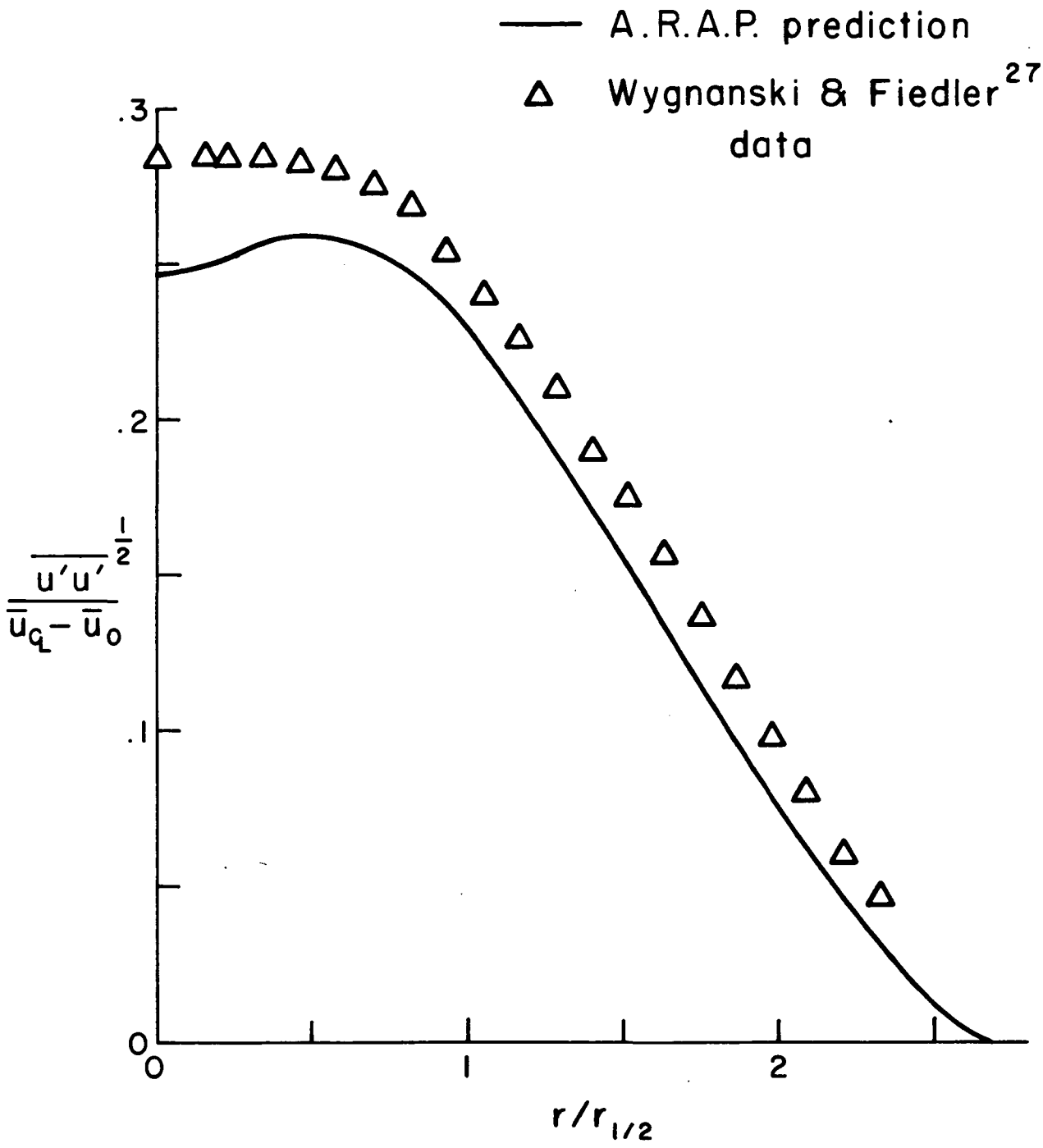

Figure 3. Profile of the axial velocity fluctuations in a free jet in the similarity region.

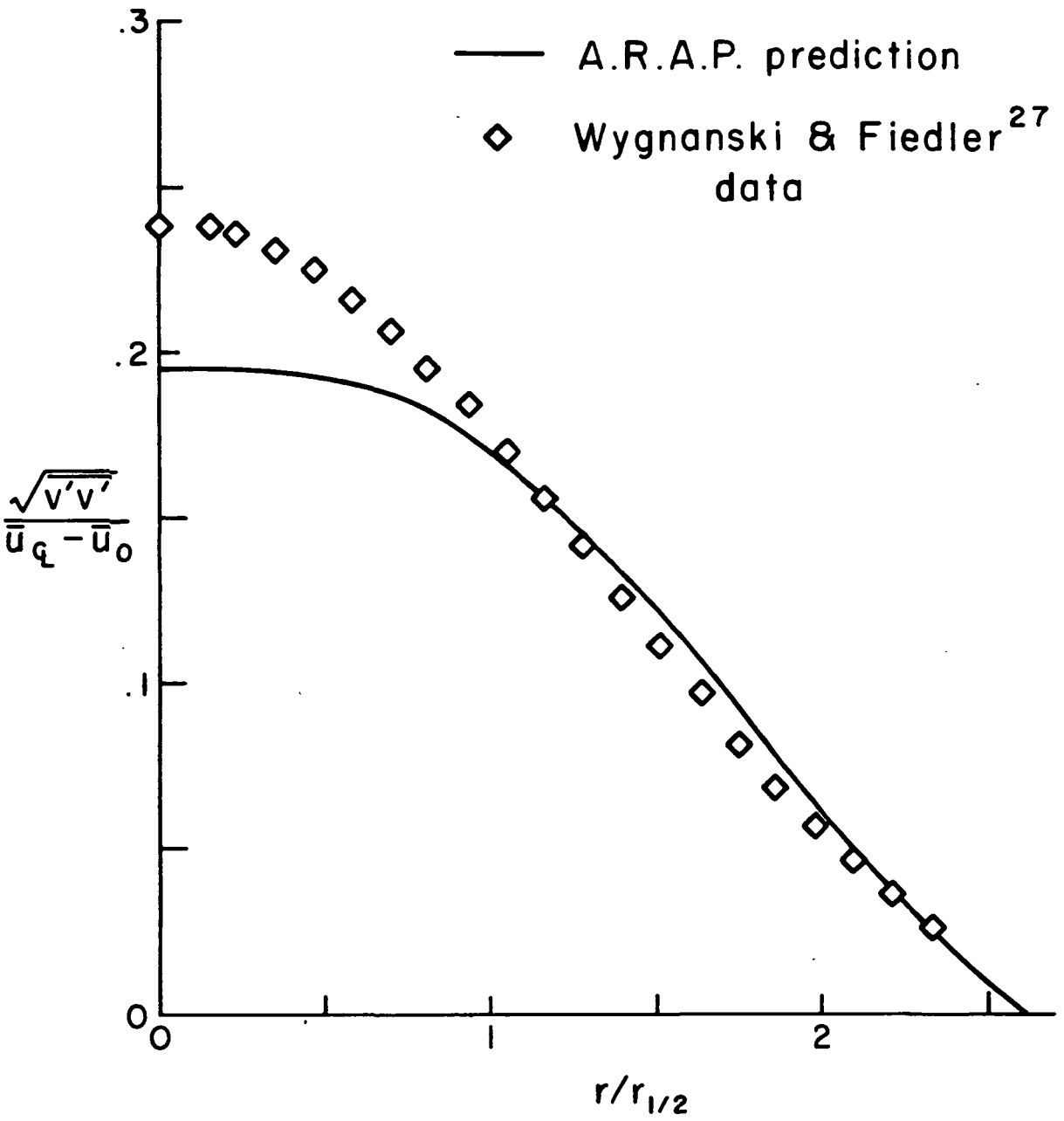

Figure 4. Profile of the radial velocity fluctuations in a free jet in the similarity region.

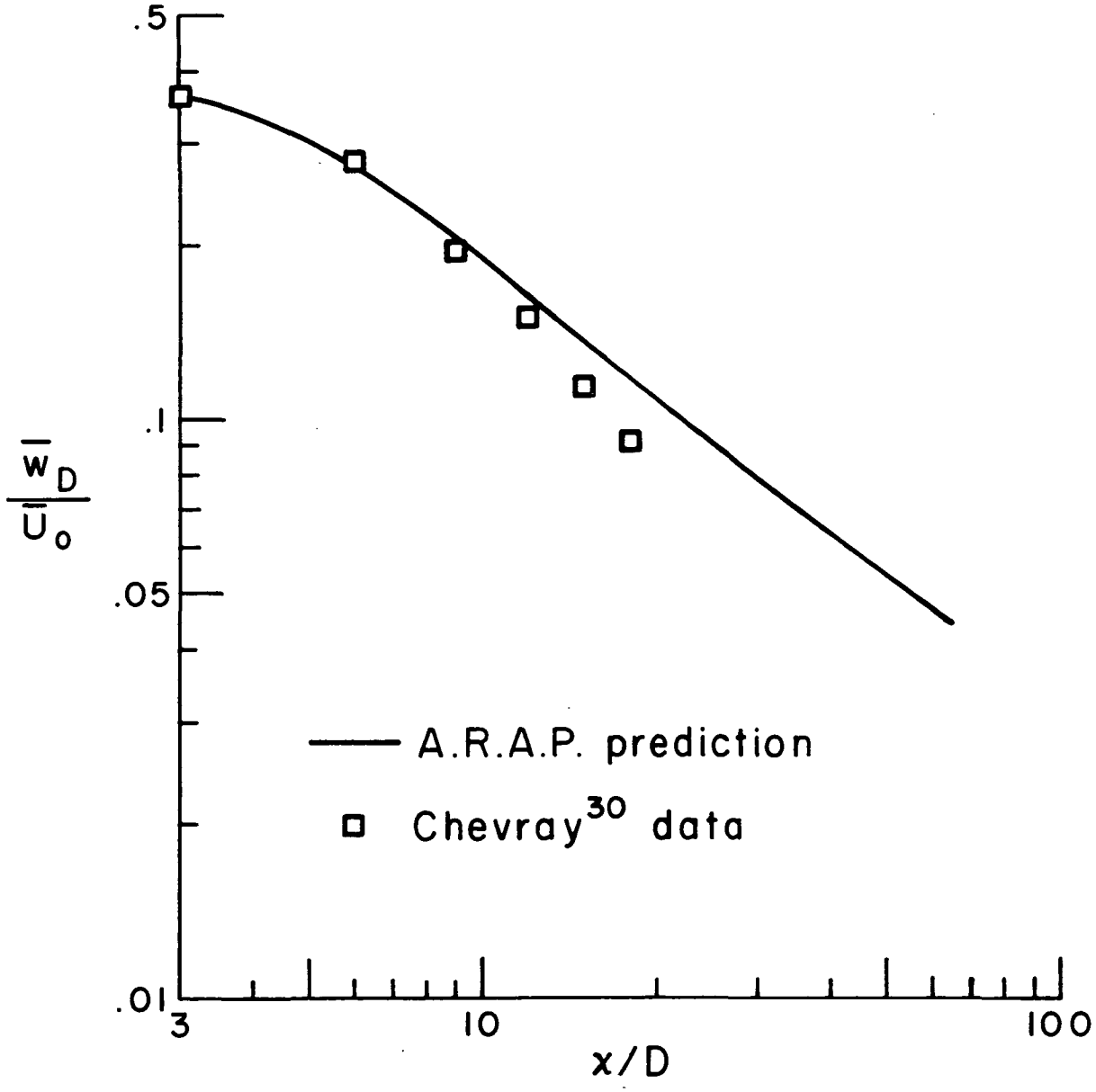

Figure 5. Variation of the mean velocity defect with distance downstream of the body.

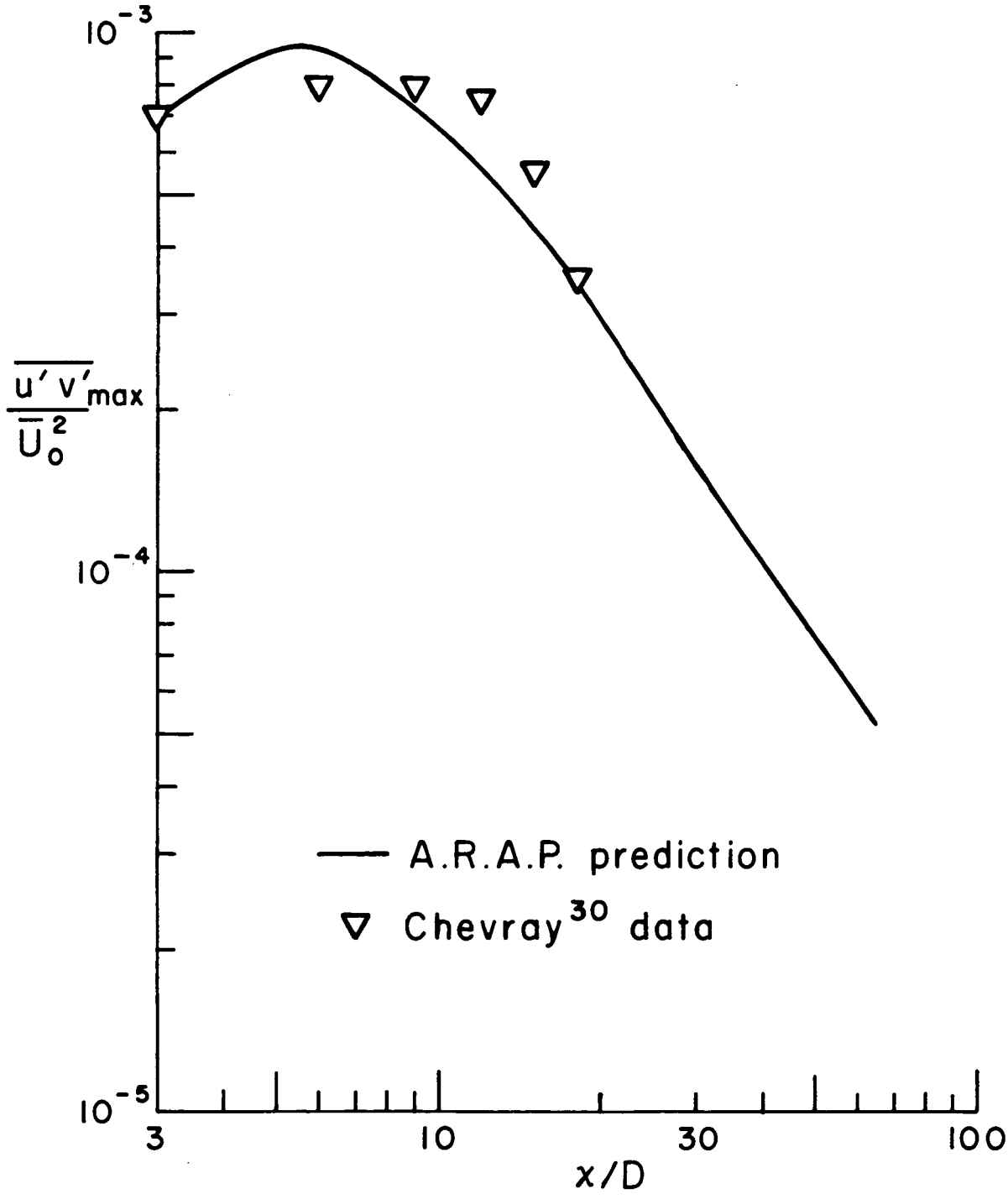

Figure 6. Axial variation of the maximum shear stress.

ments in Figures 7 and 8, and show good agreement. Previously reported calculations of this flowfield using a dynamic scale equation (ref. 17) have shown somewhat better agreement with the data. The RSL calculations using a constant scale Λ are again consistent with previous (ref. 29) A.R.A.P. calculations using an incompressible program, and verify the operation of the reacting shear layer (RSL) program.

The RSL program has been similarly checked for other flow configurations in previous publications, for example, flat plate boundary layers (ref. 22), two-dimensional jets and wakes (ref. 26), etc.

Uniform Density Shear Layer Mixing of Two Species

Recent measurements in a two-species mixing layer have been reported by Konrad (ref. 31): These measurements are part of a very elaborate and detailed study of this basic flowfield by the group under the direction of Professor Roshko at Caltech. Konrad has made measurements of the mixedness correlation $\overline{\alpha'\beta'}/\bar{\alpha}\bar{\beta}$ or $\overline{\alpha'\alpha'}/\bar{\alpha}(1-\bar{\alpha})$ in a shear layer of velocity ratio = 0.38 and consisting of two streams of different species but the same density. Figure 9 shows a comparison of the RSL program predictions for the flowfield with the experimental measurements. There is good agreement in the central turbulent region of the flowfield. The theoretical predictions for the edge regions of the flow are not symmetrical, which is somewhat surprising and is believed to be due to the difficulty of a accurately calculating the term $\overline{\alpha'\beta'}/\bar{\alpha}\bar{\beta}$ when $\bar{\alpha}$ or $\bar{\beta}$ is very small. Further, the calculations were carried out using the secondary model and the neglect of the third-order density correlations may not be justified in this flow. The calculations should be repeated with the complete "typical eddy" model. The disagreement between the theoretical predictions and the experiments may also be due to the intermittent nature of the flow and the observed large "coherent" structures. This is the only available data on this flow configuration with detailed turbulence measurements, and the comparison to the theoretical predictions to this flow have been simply included in this report as an area that requires further study. The theoretical models do not include intermittency effects at the present time.

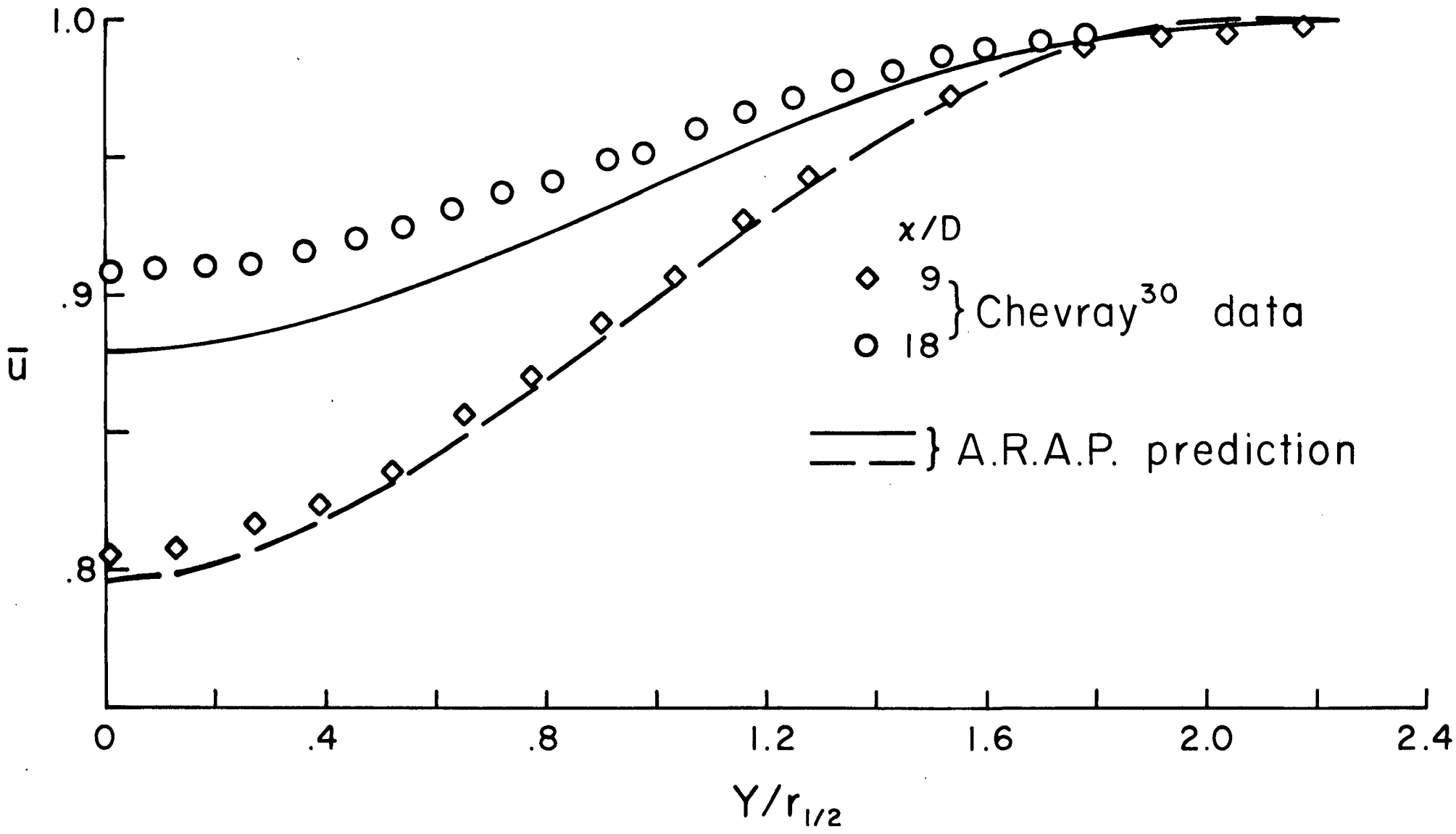

Figure 7. Mean axial velocity profiles at two axial stations in the axisymmetric wake.

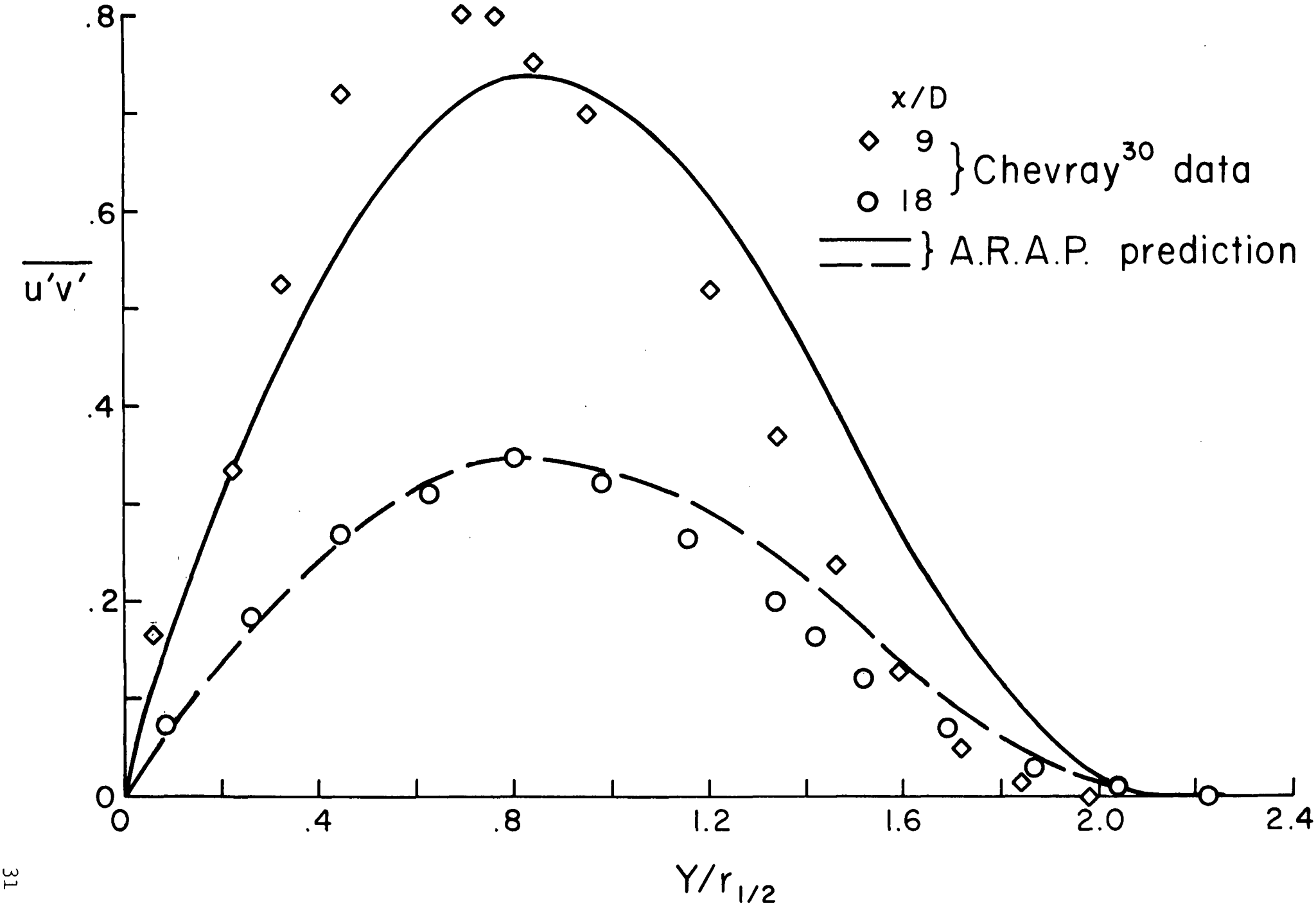

Figure 8. Shear stress profiles at two axial stations in the axisymmetric wake.

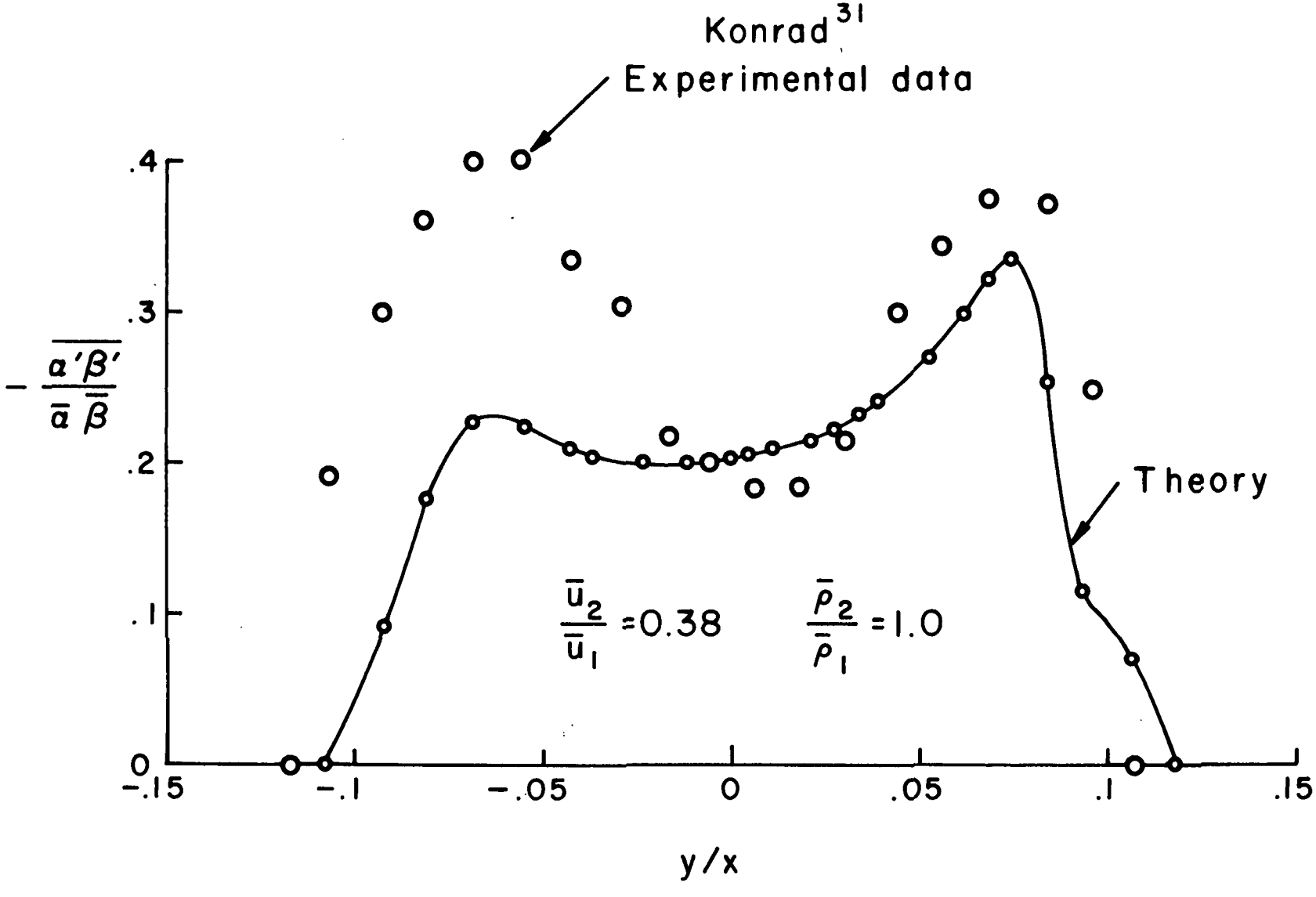

Figure 9. Profile of the unmixedness correlation $\left(-\frac{\overline{\alpha'\beta'}}{\bar{\alpha}\bar{\beta}}\right)$ in a shear layer.

Conclusions

The most important feature that must be pointed out is that all these computations and others that have been referenced, have been carried out with basically the same set of model parameters. The results demonstrate that our second-order closure techniques can predict the mean flow and details of the turbulence correlations for a wide class of nonreacting flows and provide a level of confidence in the use of these models and the programs in a predictive capacity for other flows. The details of the specific agreement with one particular experiment are not as important in this effort as the approach to the development of a universally valid model. The reacting shear layer (RSL) program is, therefore, at least correct for these limiting cases and now provides the capability to study multi-species mixing and reacting flows. Tests now have to be carried out on these flows to verify the rest of the program and to verify the models developed for the scalar correlations. This effort is now underway. Computations are being carried out for two species shear layer mixing (the initial preliminary results were shown previously in this section), hydrogen-air diffusion flames (see next section), DF chemical lasers (ref. 10), and erosive burning of solid propellants (ref. 32). However, this work is just beginning and many tests and comparisons remain to be made to thoroughly check the models and the programs.

STUDIES ON HYDROGEN-AIR DIFFUSION FLAMES

There are at the present time very few detailed measurements in turbulent reacting flows which can be used to test the assumptions and the models in a complete second-order closure analysis. Measurements are required for various second-order correlations and especially the scalar correlations and the scalar probability density functions to guide the development of these more sophisticated turbulence models for reacting flows. These experiments are quite difficult, but many measurements of this kind are now being planned by various groups and some results should become available in the near future. At present, the only systematic set of data for testing theoretical models are the detailed measurements of Kent and Bilger (ref. 11) on laboratory hydrogen-air diffusion flames. The A.R.A.P. reacting shear layer (RSL) program has been used to study this flowfield.

A schematic of the Kent-Bilger experimental setup is shown in Figure 10. The measurements of temperature, velocity, and species compositions were carried out in a coaxial mixing system consisting of a 7.62 mm diameter hydrogen-jet exhausting into an air stream flowing through a 305 mm square cross-sectional tunnel. The flame was initiated by a spark. Measurements were reported

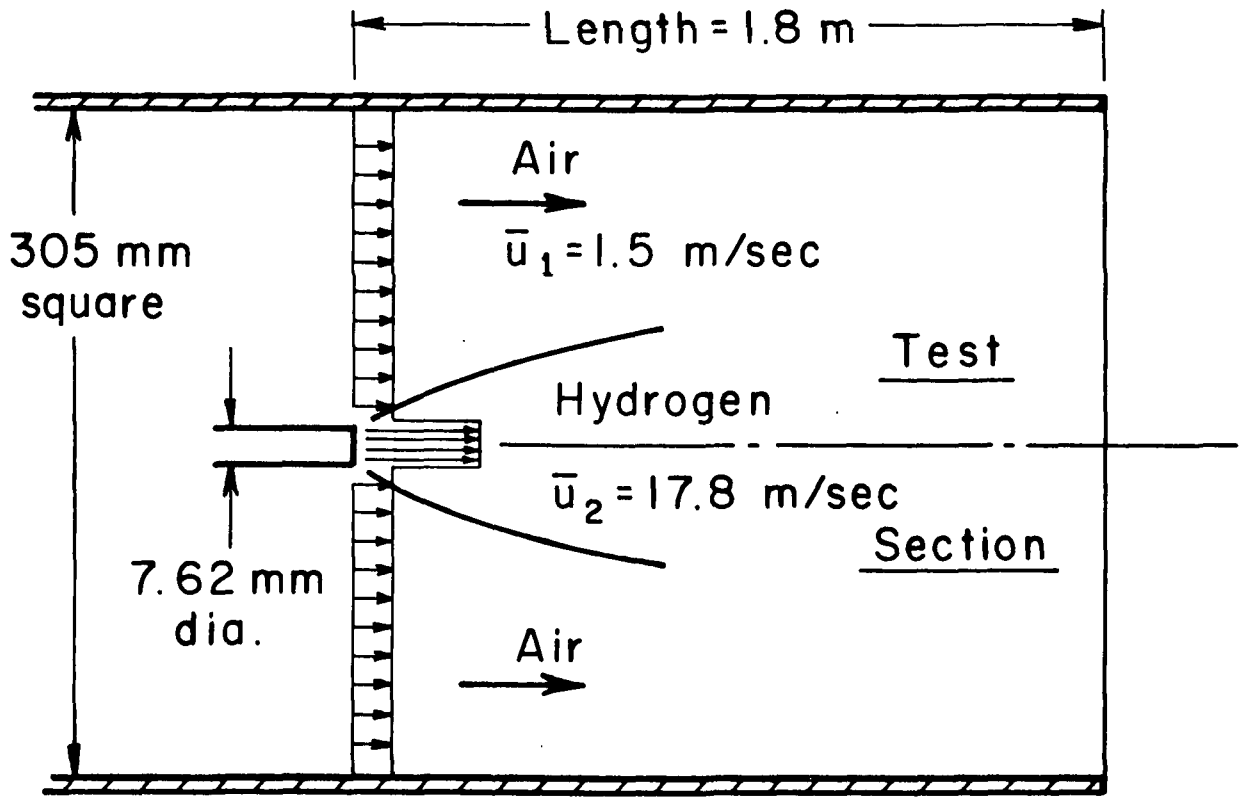

Figure 10. Kent-Bilger experimental set-up.

at nominal jet to external stream velocity ratios of 2, 5, 8, and 10. The most extensive measurements were for a velocity ratio of 10 and the theoretical calculations have been made for only this case. The actual velocity ratio for the measurements was 11.8. The measurements indicate the presence of a fairly strong axial pressure gradient. Rhodes et al. (ref. 3) have shown the important effect of the pressure gradient on the mean velocity field. Although the RSL program has the capability of imposing an external pressure gradient (for example, on a boundary layer flow) at the present time, the program does not treat a confined flow in a consistent manner. This capability will be added in the near future. For the calculations reported herein, the axial pressure gradient was neglected. The effect of the inclusion or the neglect of the pressure gradient on the predictions of the temperature and the mean species profiles is not known.

Measured velocity profiles at the nozzle exit plane were available, but to avoid the initial steep boundary layer profiles, the RSL calculations were started at $x/D = 6$. The flow properties for all the mean variables at this axial station were obtained from a NASA Langley computer program which uses a two-equation turbulence model. This code generated the profiles given in Figure 11, which were the initial conditions for all the calculations discussed here. A narrow spot of turbulent velocity correlations $\overline{u_i'u_j'}$ was introduced at the initial station with amplitude of $\overline{u'u'} = \overline{v'v'} = \overline{w'w'} = 2\overline{u'v'} \approx .01\ \Delta\bar{u}^2$. All the other second-order correlations were set zero at the initial station.

A number of different program assumptions were investigated as part of the studies on the Kent-Bilger hydrogen-air diffusion flame . As most of the measurements were in the far downstream region of the flow, a simpler and faster "superequilibrium" procedure (ref. 18) was used to calculate the species correlations in a number of the test runs. In this procedure, the transport equations for the species correlations are not solved, but instead, the species correlations are calculated from algebraic relations obtained by balancing the production and dissipation terms in the complete transport equations. The convective and diffusive terms in the equations can be assumed to be small in the downstream region of the flow. The species correlations can then be written in terms of the mean flow variables, and have the form,

$$\overline{\alpha'\phi'} = C_\phi \Lambda^2 \frac{\partial \bar{\alpha}}{\partial y} \cdot \frac{\partial \bar{\phi}}{\partial y}$$

where ϕ may be any variable (β, u, h, ρ, etc.) and C_ϕ is a constant that can be evaluated from the turbulence model parameters. In the studies discussed in this report the superequilibrium procedure was used only for the species correlations. Other turbulence correlations can also be evaluated with the use of the superequilibrium assumption. This aspect of the investigation should be studied in the future. The results of such superequilibrium calculations have to be compared to results obtained by use

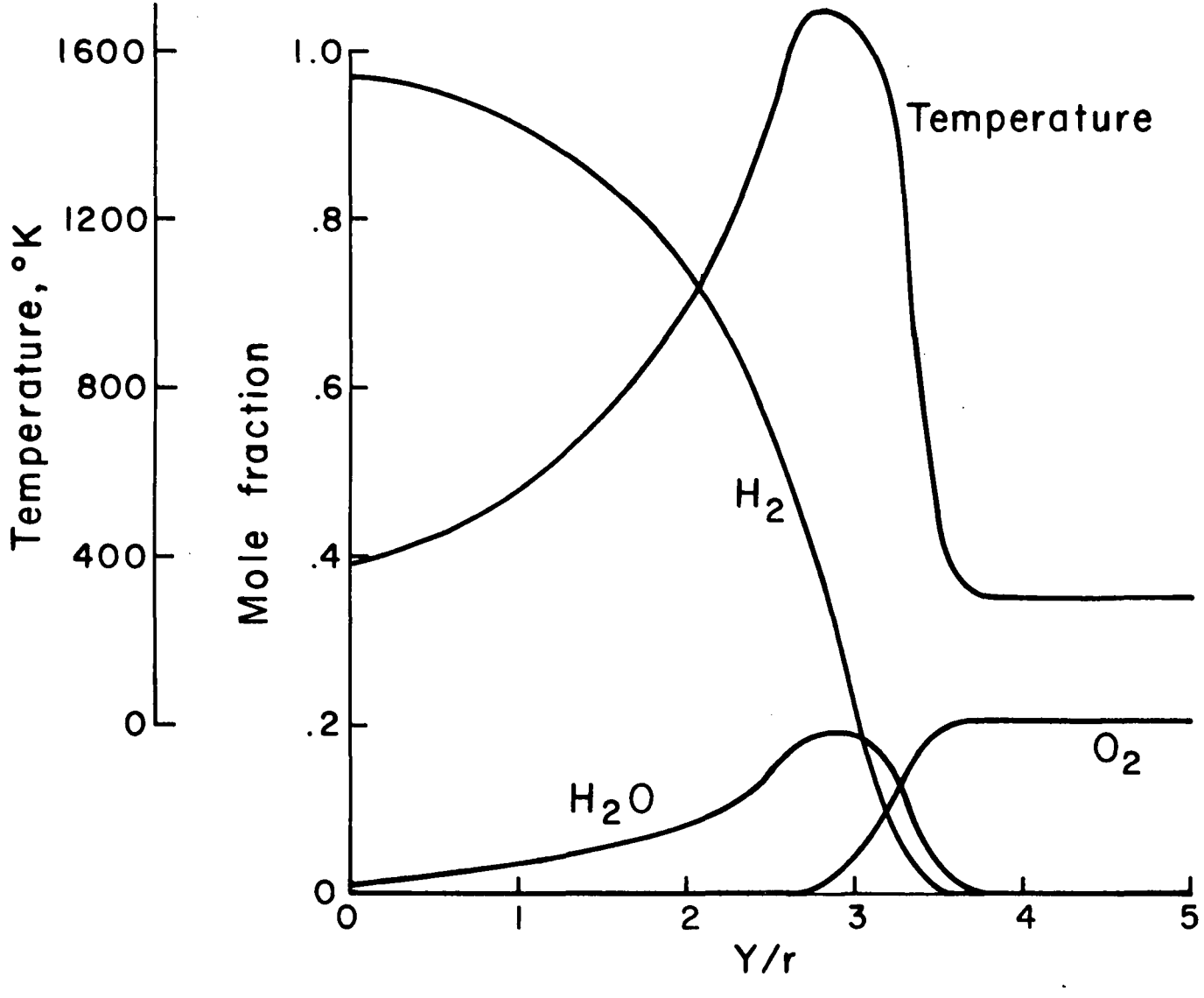

Figure 11. Initial conditions for A.R.A.P. calculations $\left(\frac{x}{D} = 6.\right)$.

of the transport equations for all the correlations which is the normal mode of program operation. Such a comparison was attempted here, but was not completed due to problems which are discussed later in this section.

The turbulent macroscale Λ was calculated from the mean axial velocity profile for the hydrogen-air diffusion flame calculations. In a reacting flowfield, the profile of scalar variables, for example, the mean temperature is quite different from the mean velocity profile. Therefore, it is quite likely that the turbulence macroscales for different variables will also be different. However, there is no convenient procedure to accurately determine these different scales at the present time and all other analyses use the same scale for all the variables. At the present time A.R.A.P. is engaged in formulating a new and consistent procedure for determining these scales. In general, the scales for different variables will be different and will vary across the flowfield.

The effect of the different scales was investigated in a very simple manner in the Kent-Bilger studies. Two cases were considered. In one, the scales for all the variables were the same and the scale was evaluated from the mean axial velocity profile. This scale is constant across the flowfield, but varies with the profile in the flow direction. In the second case, the scale for all the scalar variables is set equal to one-half the scale for all the turbulent velocity correlations. The 1/2 figure is an arbitrary estimate from the profile shapes at the initial station. The 1/2 ratio is maintained for the entire flowfield and is likely to be in error, but a more complicated formulation did not appear justified at this time. The detailed scale equation formulation currently underway should lead to a better understanding of the physics of the problem and then a more appropriate selection of the scales may be possible. Thus, in the current studies we investigated,

$$\text{(i)} \quad \Lambda_{scalar} = \Lambda_{\bar{u}}$$

$$\text{(ii)} \quad \Lambda_{scalar} = 1/2\ \Lambda_{\bar{u}}$$

All the calculations used the secondary model for the scalar correlations. The calculations using the complete "typical eddy" model with the density correlations will be done later after the complete model is incorporated into the RSL program.

The chemical rate constants used for the multi-step hydrogen-air chemistry are listed in Table I. These are in general agreement with the rates used by other investigators (refs. 3,33).

There is one additional empirical parameter that has to be specified in the current reacting runs using the RSL program. This is the limiting value for the unmixedness correlation in the chemical source term. The mean chemical source term for the

elementary reaction $\alpha + \beta \xrightarrow{k} \gamma$ can be written as,

$$\bar{\dot{w}}_\alpha = \bar{k}\bar{\rho}^2\bar{\alpha}\bar{\beta}\left[1 + \frac{\overline{\rho'\rho'}}{\bar{\rho}^2} + 2\frac{\overline{\alpha'\rho'}}{\bar{\alpha}\bar{\rho}} + 2\frac{\overline{\beta'\rho'}}{\bar{\beta}\bar{\rho}} + \frac{\overline{\alpha'\beta'}}{\bar{\alpha}\bar{\beta}}\right] + k' \text{ terms}$$

The total set of correlations inside the square brackets are termed the unmixedness correlation. For an infinitely fast reaction rate, the unmixedness correlation = -1. and the species α and β cannot coexist on the molecular scale. This is the limiting value for $k = \infty$. However, for large k, the unmixedness correlation approaches -1, but is not equal to it. In principle, the unmixedness correlation for large k can be calculated by solving the transport equations for the individual correlations. However, this procedure is subject to errors when the reaction rate is fast and it becomes necessary to calculate the limiting value of the unmixedness correlation by some different procedure. A fast chemistry limit has been derived for constant density reacting flows (see Appendix B) and the procedure is being extended to exothermic, variable density reacting flows. Alternately, the limiting value can be input as an empirical parameter. In the current set of calculations for the Kent-Bilger hydrogen-air diffusion flame studies, the alternate procedure of an empirical limiting value has been used. The unmixedness correlation is calculated at every point in the flow using the transport equations or the superequilibrium procedure. If the value of the unmixedness is smaller than the limiting value, it is set equal to the limiting value at that point in the flowfield. In the hydrogen-air diffusion flame problem, the reaction rates are very fast and the limiting values of the unmixedness correlation were found to be of the order of -0.996 to -0.999. Thus, the net turbulent reaction rate is only a very small fraction (.001 to .004) of the reaction rate that would be predicted if the effects of the turbulence were neglected and the flow was assumed to be molecularly mixed. It is, therefore quite obvious that the turbulence-chemistry interaction is of great importance here. However, due to the fast reaction rates of this problem, it is difficult to accurately compute the unmixedness correlation from the basic transport equations. The calculation of the unmixedness effects will be considerably simpler for slower reaction systems, as the need for extreme accuracy in the numerical solution of the transport equations for the correlations will be obviated.

The results obtained for $\Lambda_{scalar} = \Lambda_{\bar{u}}$ are considered first. Figures 12 and 13 compare the results for the temperature and species profiles for the RSL predictions with the Kent-Bilger measurements at x/D = 40. The calculations use the superequilibrium procedure and use an unmixedness limit of -0.9995. The peak temperatures are in reasonably good agreement but the calculated temperature profile is significantly wider than the measured profile

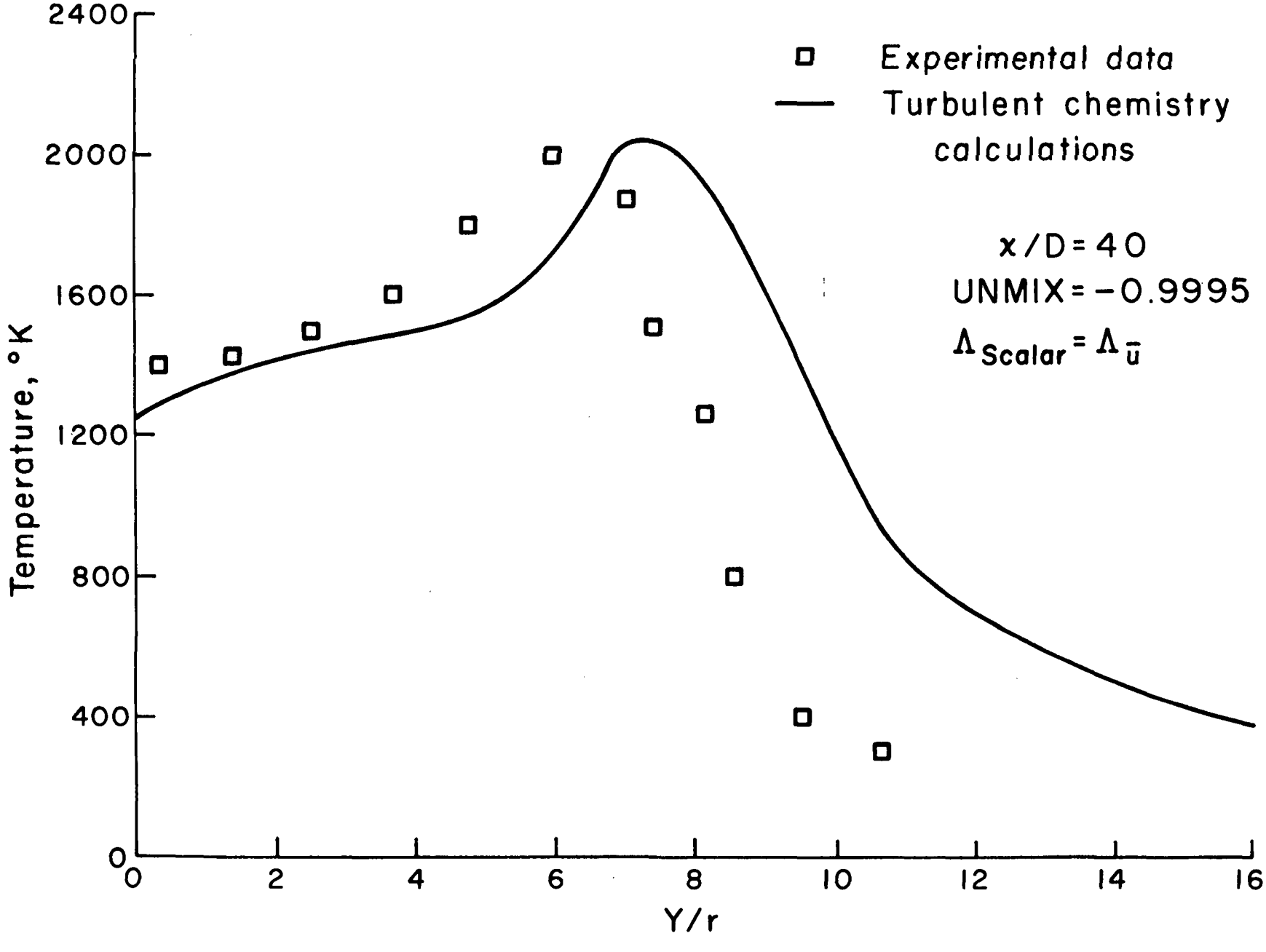

Figure 12. Mean temperature radial profile in hydrogen-air diffusion flame. Secondary model. Superequilibrium procedure.

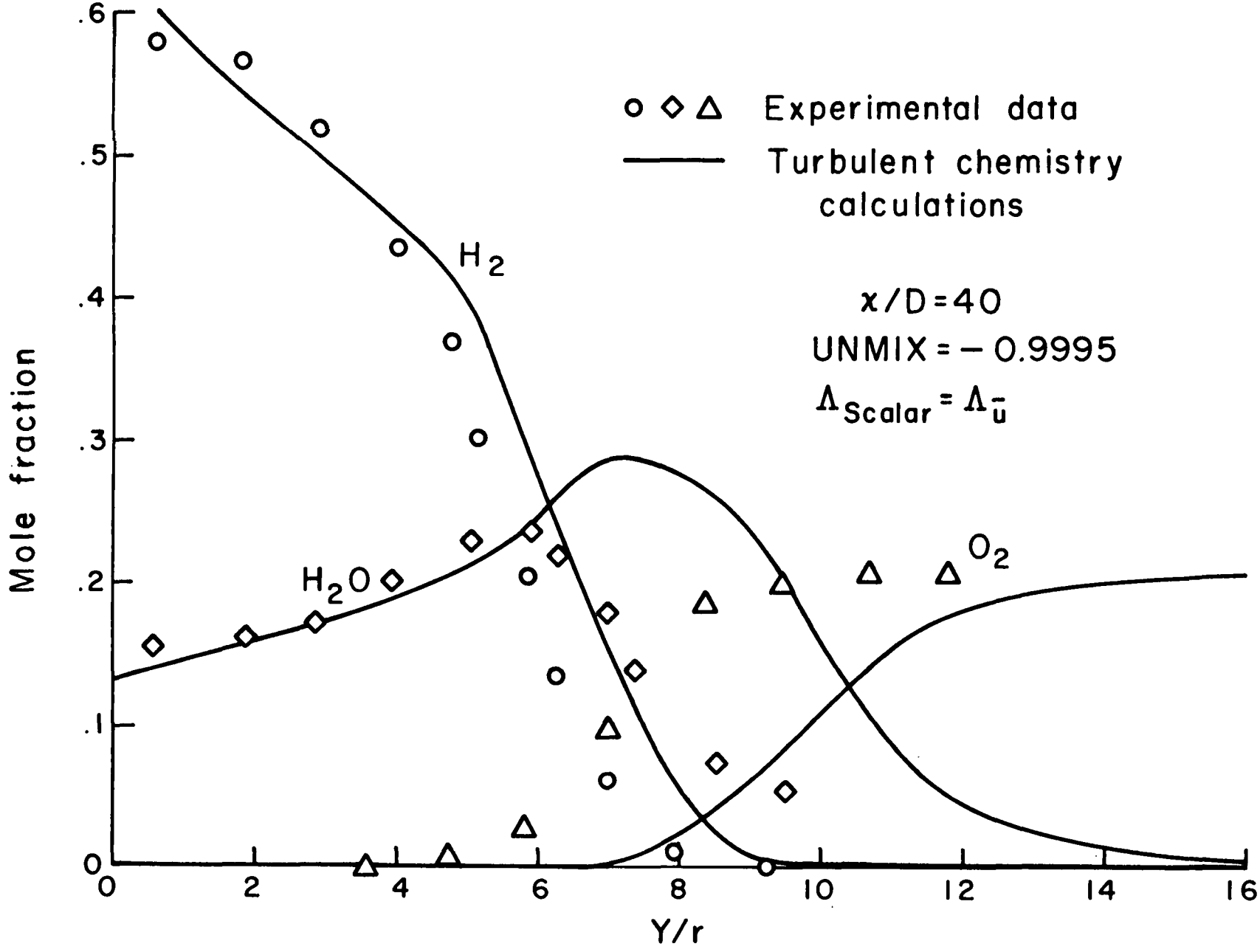

Figure 13. Mean species radial profile in hydrogen-air diffusion flame. Secondary model. Superequilibrium procedure.

at this position. The species profiles also show that the flame location is predicted at a somewhat larger radius than in the experiments. The shape of the oxygen profile is steeper in the measurements but the hydrogen profile is not too different if one compensates for the difference in flame location. The measured flame thickness (region of overlap of hydrogen and oxygen) is larger than the predictions which suggests that the unmixedness limit should be set even closer to -1 . Computations made with the limit set at -.998 and -.999 predicted even smaller reaction zone thickness. The results at x/D = 80 are shown in Figures 14 and 15 and the same comments apply although the profile shapes for the temperature and the oxygen are now in better agreement with the data.

To show the importance of including the turbulence-chemistry interaction effects, a computation was attempted using a "laminar chemistry" formulation. In this case the unmixedness correlation is completely neglected in the calculation of the reaction source terms and the flow is assumed to be perfectly mixed on the molecular scale. Then, $\bar{\dot{w}}_\alpha = \bar{k}\bar{\rho}^2\bar{\alpha}\bar{\beta}$, and is analogous to the source term for laminar flow which is the reason for the name used for this approach. Unfortunately, the run gets into severe problems with the prediction of very large values of $\overline{h'h'}$ and consequent errors in the calculation of the mean temperature and density, and the comparison could not be made for $\Lambda_{scalar} = \Lambda_{\bar{u}}$ case.

A test calculation which does not use the superequilibrium assumption for the species correlations was also attempted, but was not successful due to problems in the multi-step chemistry procedure. The forward step size in the computation becomes very small due to backups in the minor species diffusion and chemistry calculations and the computation could not be completed. This problem can be corrected but up to now we have not been able to devote the necessary effort.

The problems experienced in the "laminar chemistry" run for $\Lambda_{scalar} = \Lambda_{\bar{u}}$ (too large $\overline{h'h'}$) and the predicted large profile widths for the temperature and the species in the "turbulent chemistry" runs suggested that the macroscale for the scalar quantities probably should be smaller. As discussed before, on the basis of the initial profiles of the variables, we selected $\Lambda_{scalar} = 1/2\ \Lambda_{\bar{u}}$ to make a series of test computations for the Kent-Bilger diffusion flame studies.

Figures 16 and 17 compare the program predictions to the measurements at x/D = 40 for this scale assumption. The calculations used the superequilibrium assumption. The unmixedness correlation limit is set at -.9963 after a number of tests. The results are quite sensitive to the choice of the limit as is shown

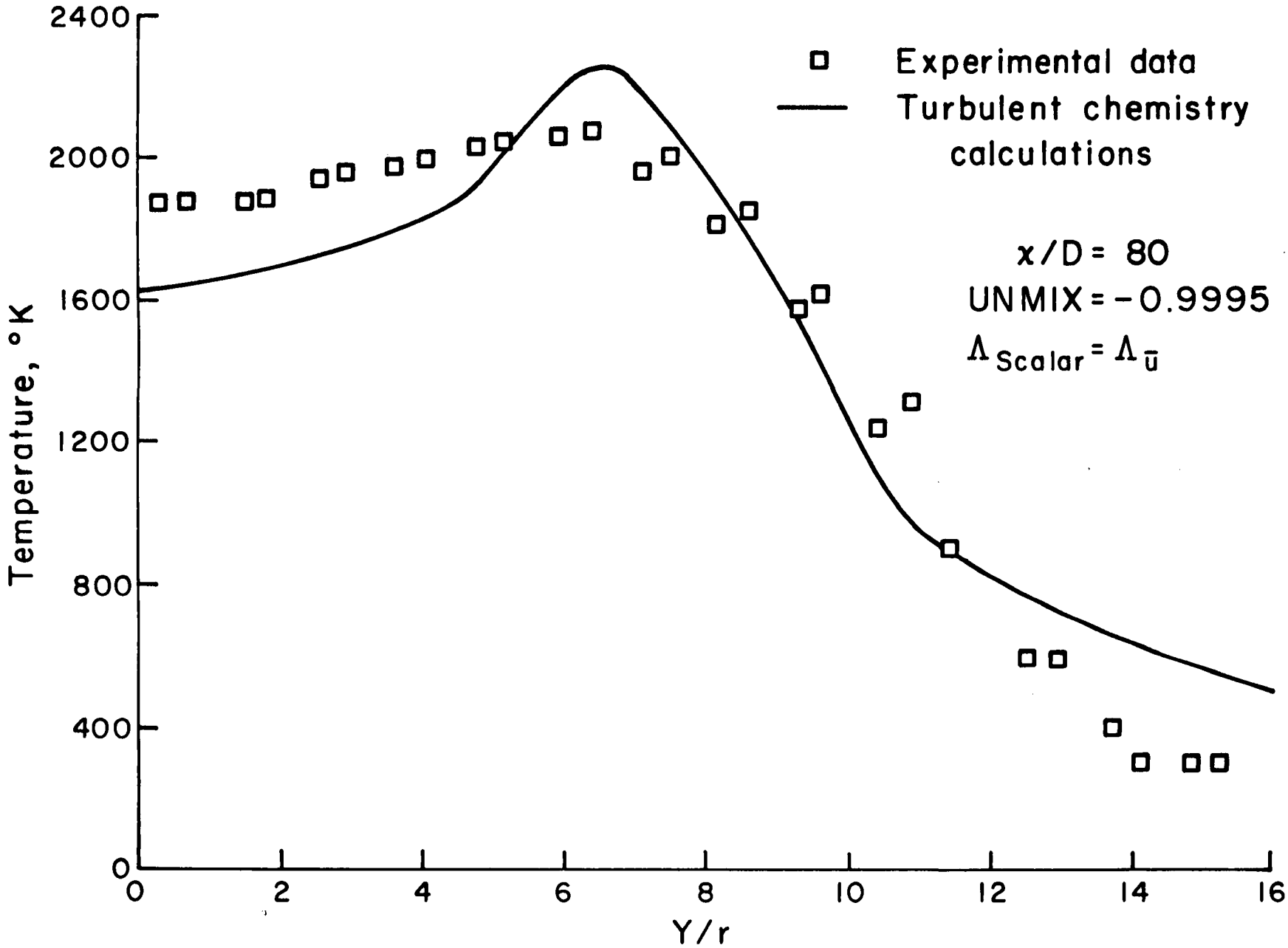

Figure 14. Mean temperature radial profile in hydrogen-air diffusion flame. Secondary model. Superequilibrium procedure.

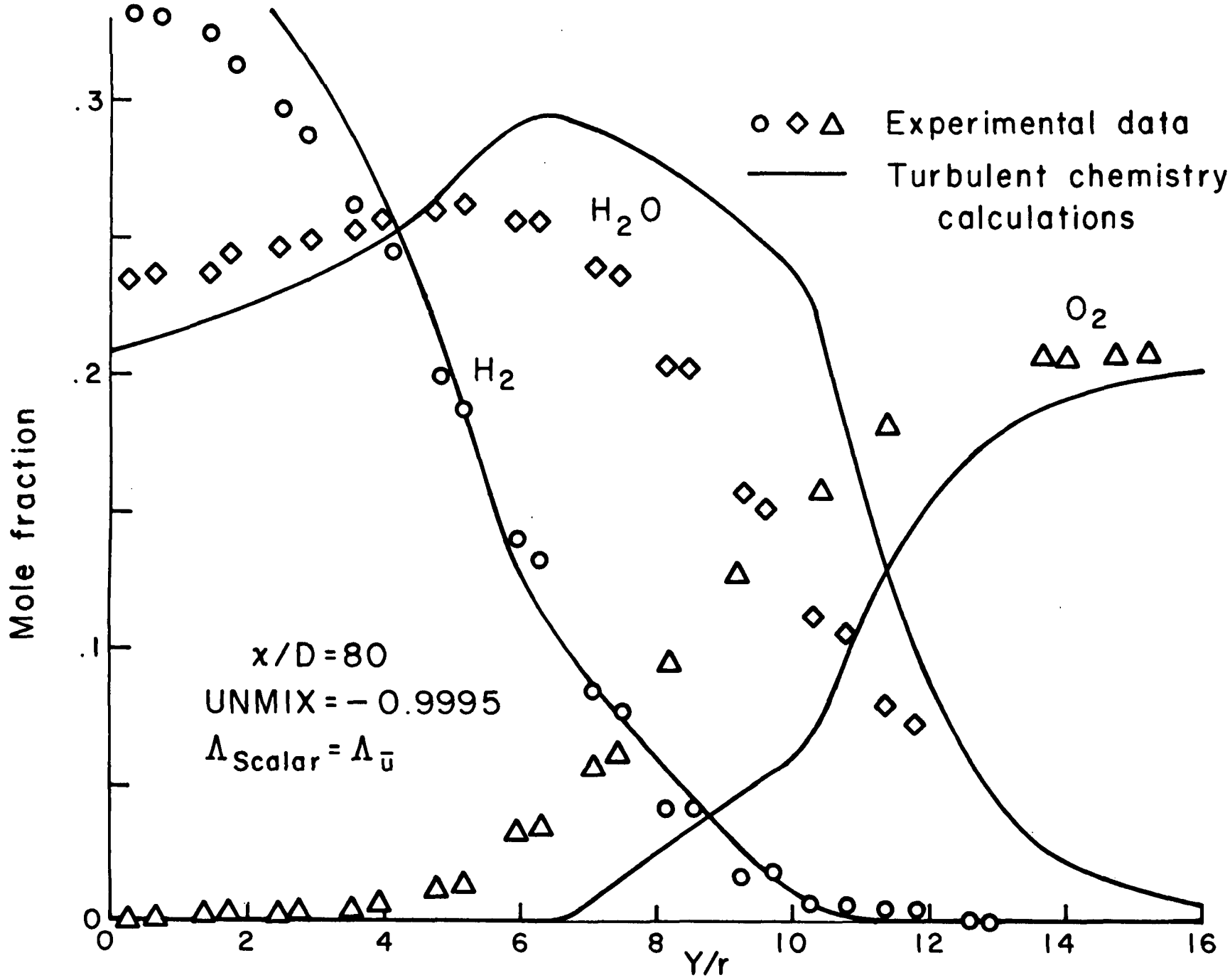

Figure 15. Mean species radial profile in hydrogen-air diffusion flame. Secondary model. Superequilibrium procedure.

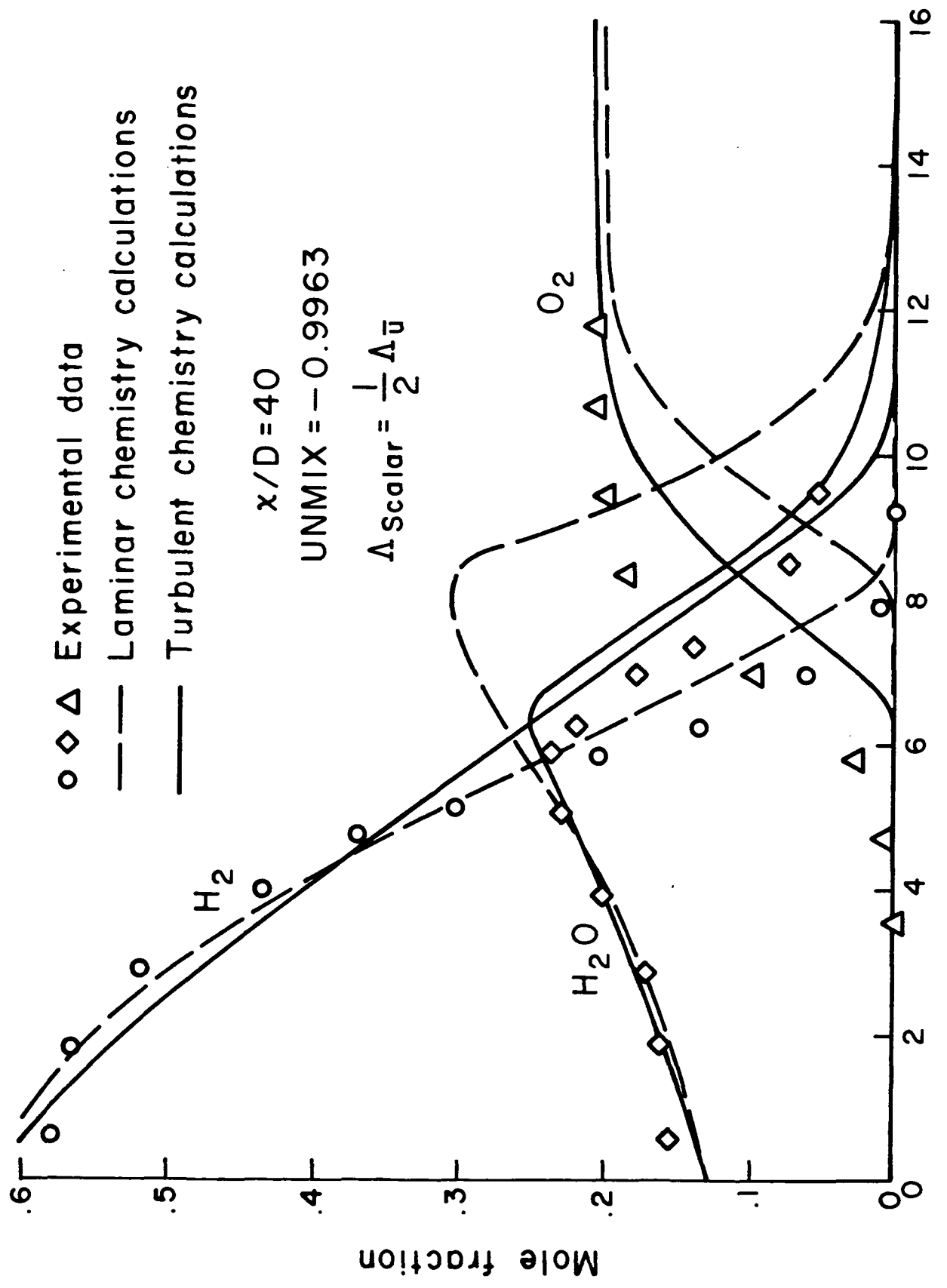

Figure 16. Mean species radial profile in hydrogen-air diffusion flame. Secondary model. Superequilibrium procedure.

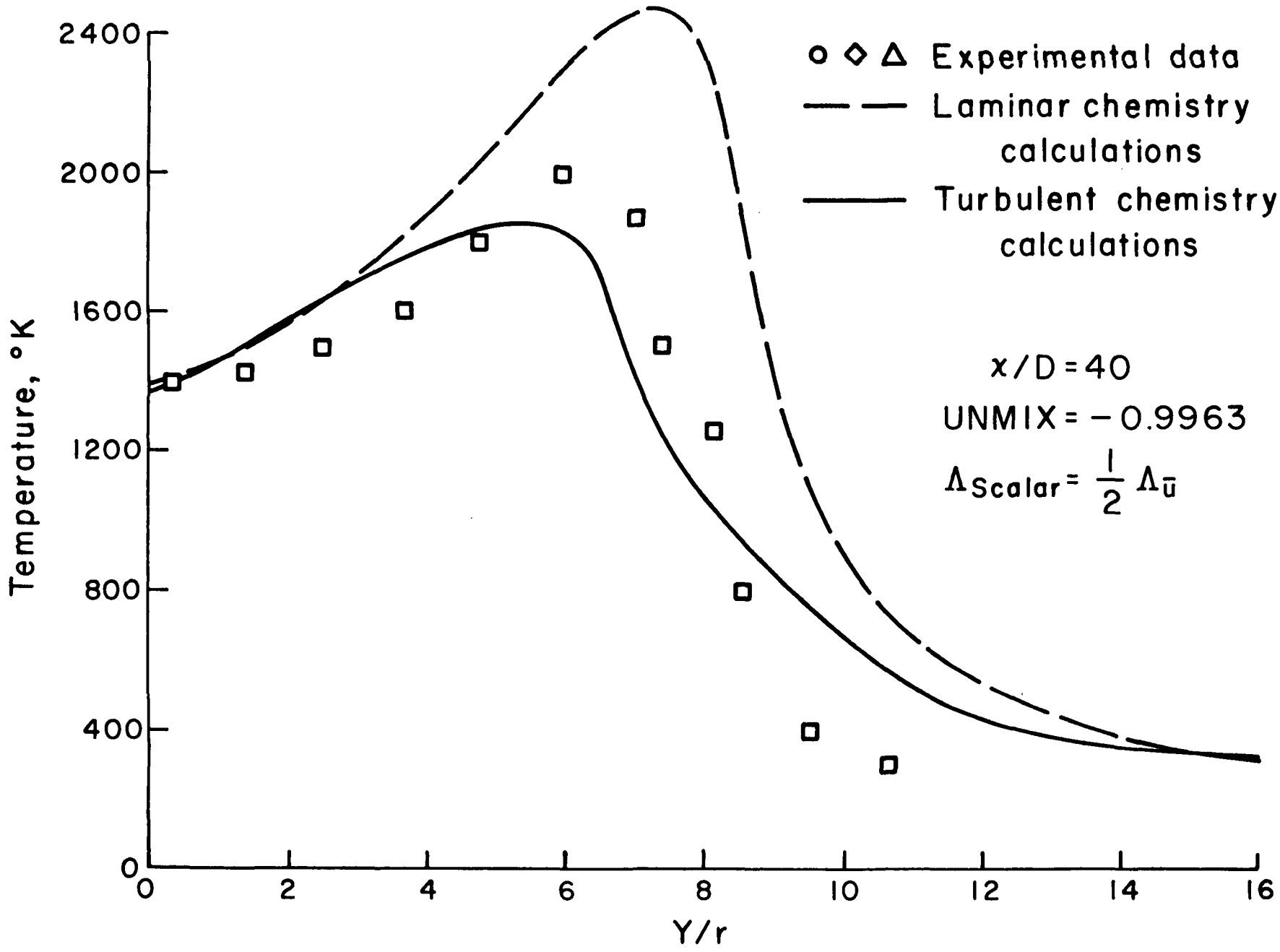

Figure 17. Mean temperature radial profile in hydrogen-air diffusion flame. Secondary model. Superequilibrium procedure.

later. Figure 16 shows the results for the mean species with the use of both the "laminar chemistry" (perfect mixing) and the "turbulent chemistry" formulations. It is quite clear that there is much better agreement with the experimental data with the inclusion of the scalar correlations in the reaction source terms. When the species and density fluctuations are neglected in the "laminar chemistry" approximation, the flame thickness is very small. The turbulence-chemistry interaction effects have to be included to correctly predict the observed turbulent flame thickness. However, there still is significant disagreement between the computer predictions and the data. The predicted flame position is at a larger radius than the measurements indicate and the overlap between the hydrogen and oxygen profiles is now larger than in the experimental observations. These differences require further testing of the models and the assumptions used in these calculations, for example, the neglect of the axial pressure gradient, the macroscale assumption, the superequilibrium assumption, etc.

Figure 17 shows the results for the temperature profile. With the use of the "laminar chemistry" approximation the peak temperature is high. The use of the "turbulent chemistry" formulation predicts temperatures that are much more consistent with the experimental values, although the predictions are somewhat lower. Figures 16 and 17 clearly demonstrate that for calculations using finite rate chemistry, the significant features of turbulent diffusion flames can only be predicted when the effect of scalar fluctuations is included in the reaction source term computation. The figures also show that the RSL program predictions are in fairly good agreement with the Kent-Bilger hydrogen-air diffusion flame data at $x/D = 40$ when all the previously discussed assumptions and empirical constants are used. However, when the predictions are compared to the data at $x/D = 80$, the agreement is not satisfactory. Figures 18 and 19 show the results at this axial position. The significant disagreement is in the reaction zone thickness and in the peak temperature. It appears that the unmixedness limit should be closer to -1 at this station than at $x/D = 40$. This is not unreasonable, in fact, our studies on a simple mixing layer with chemical reaction (ref. 26) show that the unmixedness correlation asymptotically approaches -1 as x increases. However, it is difficult to incorporate this variation of the unmixedness limit in the theory at this time without additional empiricism.

Figure 20 shows the sensitivity of the predictions to the choice of the unmixedness limit. The calculations are compared at $x/D = 40$. The calculations with an unmixedness limit of -0.996 are in best agreement with the measurements at this axial position. It is seen that the unmixedness correlation has to be calculated to an accuracy of the order of 10^{-3}. The use of a fast chemistry limit may prove to be the most accurate procedure

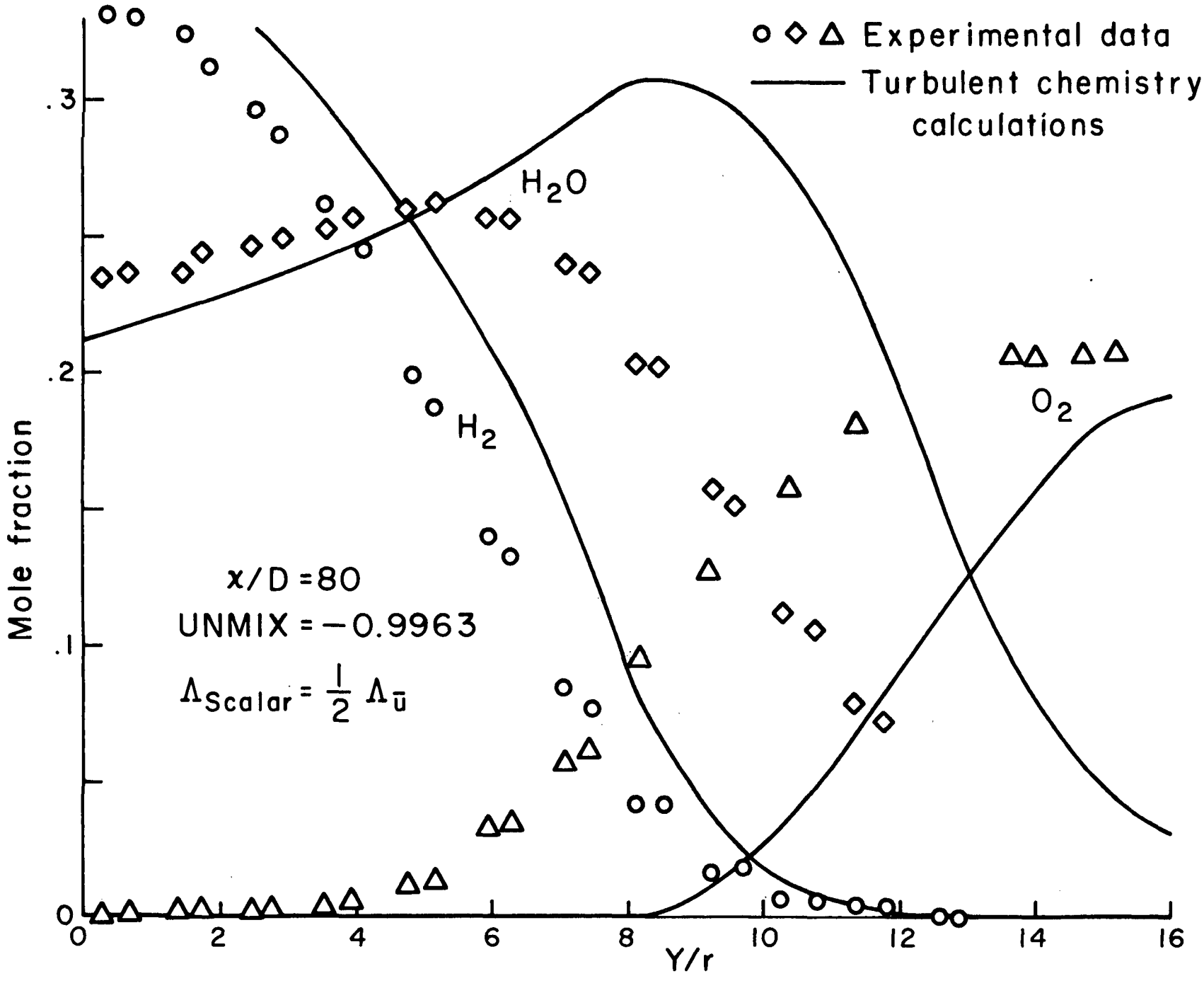

Figure 18. Mean species radial profile in hydrogen-air diffusion flame. Secondary model. Superequilibrium procedure.

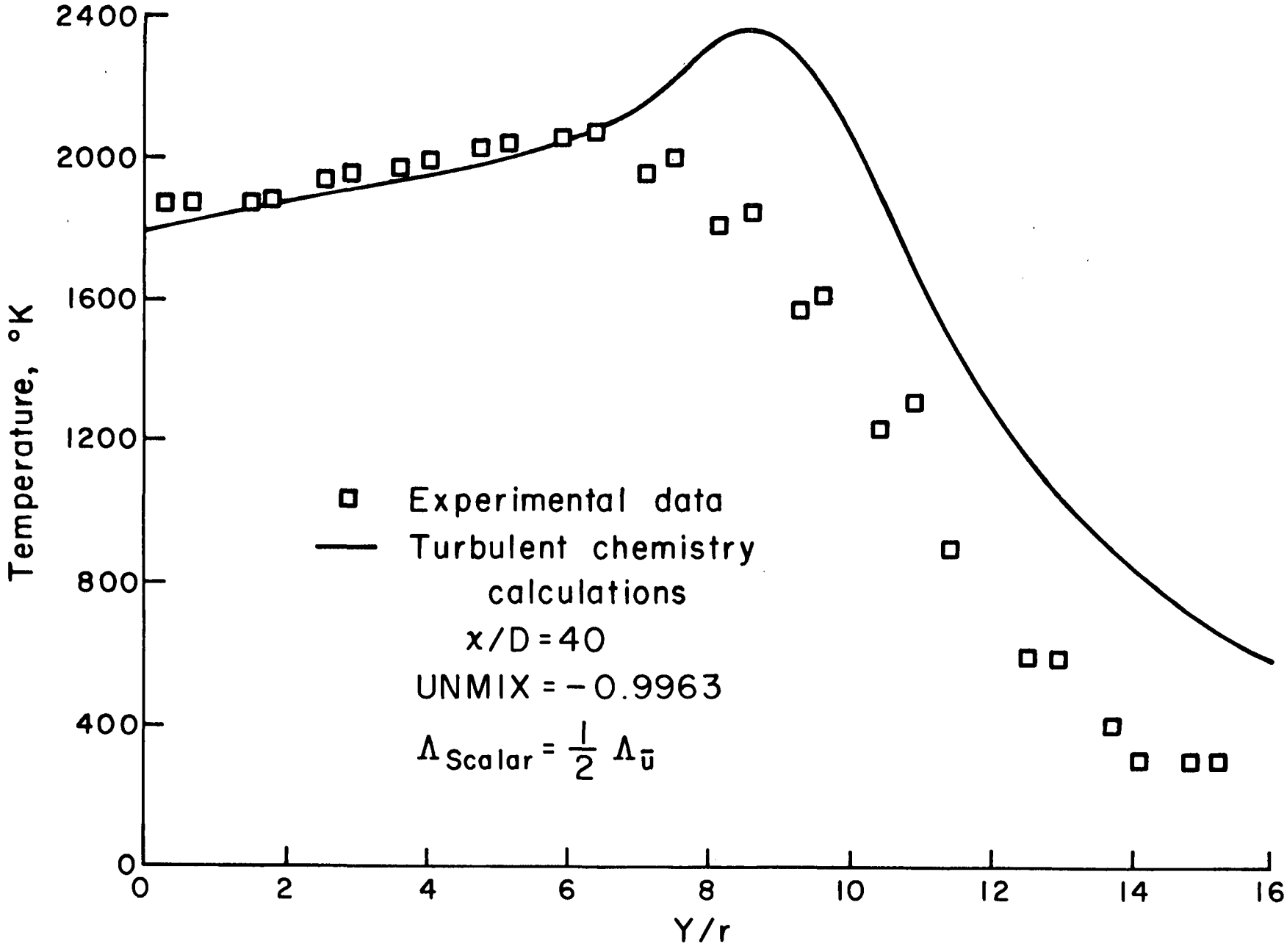

Figure 19. Mean temperature radial profile in hydrogen-air diffusion flame. Secondary model. Superequilibrium procedure.

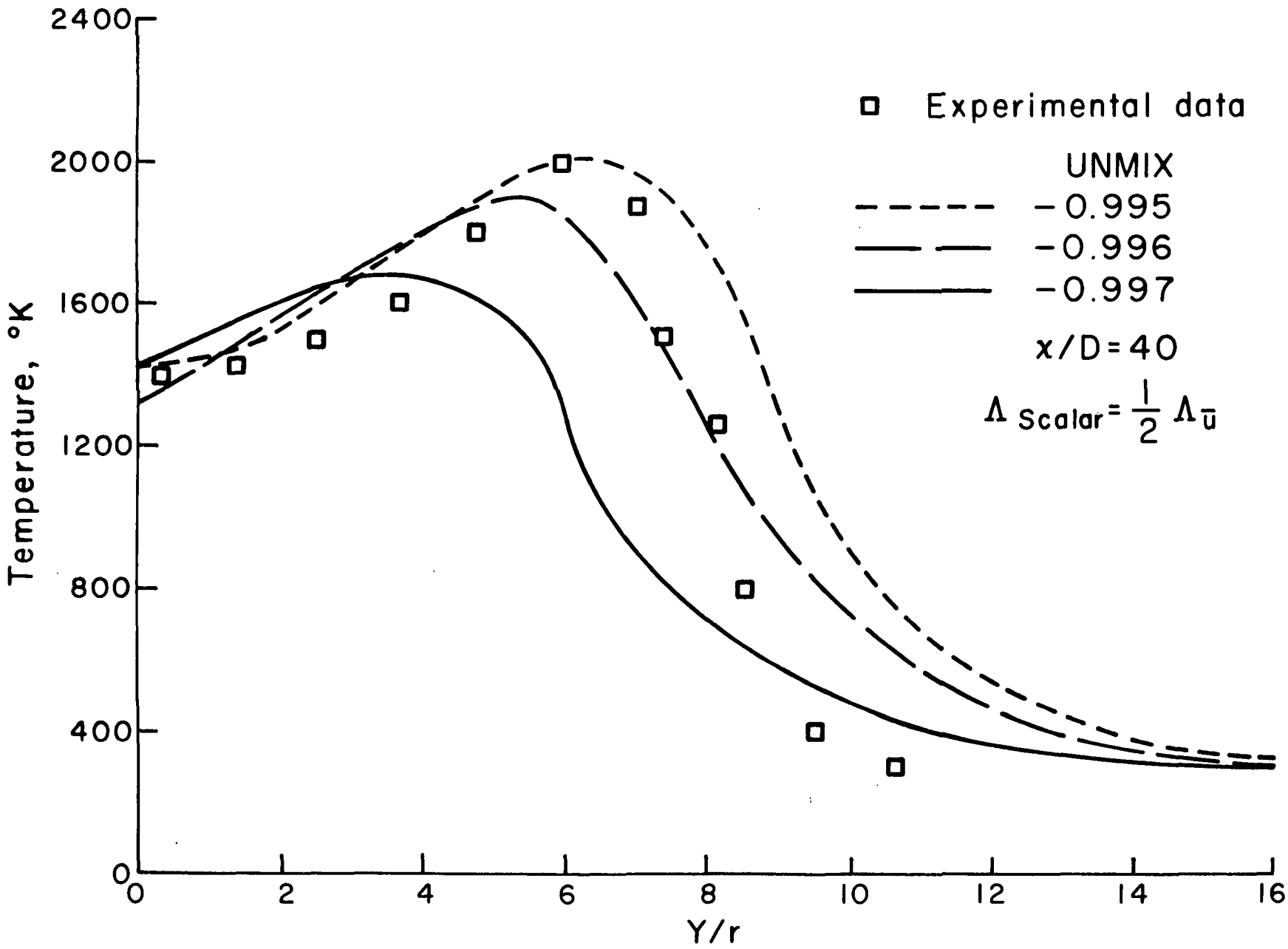

Figure 20. Sensitivity of mean temperature profiles to unmixedness limit. Secondary model. Superequilibrium procedure.

for calculating the unmixedness correlation limit for the fast hydrogen-air reactions.

In summary, the results of these calculations have demonstrated the importance of including the species and temperature fluctuation effects in calculations of turbulent diffusion flames with finite rate chemistry. These effects are included in a second-order closure analysis of the flowfield as is being developed by A.R.A.P. However, a considerable amount of work still remains to be done before one can obtain definitive comparisons between the reacting shear layer (RSL) program predictions and experimental data such as the measurements of Kent and Bilger. The importance of the selection of the correct macroscale for the scalar correlations and that for the turbulent velocity correlations has been demonstrated. The development of a scale equation formulation based on the two-point correlation function should be helpful in determining the proper scales. The empirical choice of the unmixedness limit may be avoided by the development of suitable fast chemistry limits, or it may become unnecessary when the transport equations are accurately solved with the complete "typical eddy" model. The calculations reported here with the secondary model and the superequilibrium procedure have to be repeated with the use of the full solution of all the transport equations and with the "typical eddy" model for the scalar correlations. The concept of the simplified "typical eddy" model has been successfully verified in low heat release reaction flows. However, the use of the simplified "typical eddy" model was not successful in the diffusion flame studies as substantial errors in the mean density and the density correlations occur due to their neglect in the model construction. Significant progress has been made recently toward the development of the complete model which includes the density fluctuation correlations.

SUMMARY AND CONCLUSIONS

A complete second-order closure program for the study of turbulent reacting shear flows has been developed. The program is capable of handling multi-species, multi-step chemical reactions and includes turbulence-chemistry interaction effects in the analysis. Calculations for a hydrogen-air axisymmetric diffusion flame show the importance of including the scalar correlations of species and temperature in calculating the chemical source terms for finite rate chemistry calculations. It is necessary to include the turbulence-chemistry interaction to correctly predict important features of turbulent diffusion flames such as the thick reaction zone.

The current studies used a number of assumptions and simplifications, such as the use of the superequilibrium formulation, the use of the secondary model for the scalar correlations, the arbitrary specification of the turbulent scale for the scalars, and the unmixedness limit, etc. These approximations became necessary due

to a variety of reasons. The superequilibrium assumption was used simply because of numerical problems in the multi-step chemistry code and it is probably the simplest to eliminate. The secondary model had to be used because of the inadequacy of the simplified "typical eddy" model to handle variable density flows and this assumption can only be corrected when the complete model is developed. The calculations led to the discovery that it may be necessary to specify different macroscales for scalar variables in reacting flows. This has to be examined in greater detail before a final conclusion can be reached. The possibility was anticipated in the very early model development work (ref. 18) but was not necessary in any of our previous studies. The unmixedness limit can now be calculated using the procedure derived in Appendix B. The current studies should, therefore, be considered as preliminary and have served to define a number of problem areas that need further investigation. The development of the "typical eddy" model and the questions regarding the turbulent scale specification are probably the two most important areas that will change the results of the calculations.

The A.R.A.P. reacting shear layer (RSL) program developed under this research effort is an operational program and will provide the basic capability to carry out second-order closure calculation of turbulent reacting flows. The new models developed in the future can be easily incorporated into the program. Our studies have already demonstrated some of the important effects in nonequilibrium turbulent flowfields that can only be properly analyzed with the use of a second-order closure program.

REFERENCES

1. Donaldson, C. duP.; and Hilst, G. R.: Chemical Reactions in Inhomogeneous Mixtures: The Effect of the Scale of Turbulent Mixing. Proceedings of the 1972 Heat Transfer and Fluid Mechanics Institute, Stanford University Press, Stanford, CA, pp. 256-261.

2. Spalding, D. B.: Mixing and Chemical Reaction in Steady Confined Turbulent Flames, 13th Symposium (International) on Combustion, the Combustion Institute, Pittsburgh, PA, 1971, pp. 645-657.

3. Rhodes, R. P.; Harsha, P. T.; and Peters, C. E.: Turbulent Kinetic Energy Analyses of Hydrogen-Air Diffusion Flames, Acta Astronautica, Vol. 1, 1974, pp. 443-470.

4. Bray, K. N. C.; and Moss, J. B.: A Unified Statistical Model of the Premixed Turbulent Flame. AASU Report No. 335, University of Southampton, November 1974.

5. Libby, P. A.: One Turbulent Flows with Fast Chemical Reactions. III. Two-Dimensional Mixing with Highly Dilute Reactants. Combustion Science and Technology (Special Issue on Turbulent Reactive Flows), Gordon and Breach Science Publishers, NY (in press).

6. Lockwood, F. C.; and Naguib, A. S.: The predictions of the Fluctuations in the Properties of Free, Round-Jet, Turbulent, Diffusion Flames, Combustion and Flame, Vol. 24, 1975, pp. 109-124.

7. Borghi, R.; and Moreau, P.: Turbulent Combustion in a Premixed Flow. Paper presented at Fifth International Colloquium on Gasdynamics of Explosions and Reactive Systems, Bourges, France, September 1975.

8. Spalding, D. B.: A General Theory of Turbulent Combustion, the LaGrangian Aspects. Paper presented at AIAA 15th Aerospace Sciences Meeting, Los Angeles, CA, AIAA 77-141, January 24-26, 1977.

9. Kewley, D. J.: A Model of the Supersonic HF Chemical Mixing Laser Including Turbulence Effects on the Chemistry. Paper presented at D.G.L.R. Symposium on Gasdynamic and Chemical Lasers, Koln, W. Germany, October 1976.

10. Varma, A. K.; Fishburne, E. S.; Beddini, R. A.: Modeling of Turbulent Mixing and Reactions in Chemical Lasers. AFOSR-TR-77-0584, January 1977.

11. Kent, J. H.; and Bilger, R. W.: Turbulent Diffusion Flames. Fourteenth Symposium (International) on Combustion (The Combustion Institute, Pittsburgh, PA), 1973, pp. 615-625.

12. Launder, B. E.; and Spalding, D. B.: Mathematical Models of Turbulence. Academic Press, 1972.

13. Bradshaw, P.: The Understanding and Prediction of Turbulent Flow, Aeronautical Journal, Vol. 16, 1972, pp. 403-418.

14. Saffman, P. G.: A Model for Inhomogeneous Turbulent Flow, Proceedings of Royal Society of London, Vol. 317, 1970, pp. 417-433.

15. Varma, A. K.; Beddini, R. A.; Sullivan, R. D.; and Donaldson, C. duP.: Application of an Invariant Second-Order Closure Model to Compressible Turbulent Shear Layers. Paper presented at AIAA 7th Fluid and Plasma Dynamics Conference, Palo Alto, CA, June 17-19, 1974, AIAA 74-592.

16. Lewellen, W. S.; Teske, M. E.; and Donaldson, C. duP.: Turbulence Model of Diurnal Variations in the Planetary Boundary Layer. Proceedings of the 1974 Heat Transfer and Fluid Mechanics Institute, 1974, pp. 301-319.

17. Lewellen, W. S.: Use of Invariant Modeling. A.R.A.P. Report No. 243, April 1975.

18. Donaldson, C. duP.: Atmospheric Turbulence and the Dispersal of Atmospheric Pollutants. EPA-R4-73-016a, 1973.

19. Fishburne, E. S.; Beddini, R. A.; and Varma, A. K.: The Computation of Afterburning Rocket Exhaust Plumes. A.R.A.P. Report No. 283, July 1976.

20. Varma, A. K.: Second-Order Closure of Turbulent Reacting Shear Flows. A.R.A.P. Report No. 235, February 1975.

21. Lewellen, W. S.; and Teske, M. E.: Prediction of the Monin-Obukhov Similarity Functions from an Invariant Model of Turbulence, J. Atmos. Sci., Vol. 30, 1973, pp. 1340-1345.

22. Varma, A. K.; Beddini, R. A.; Sullivan, R. D.; and Fishburne, E. S.: Turbulent Shear Flows in Laser Nozzels and Cavities. A.R.A.P. Report No. 231, October 1974.

23. Donaldson, C. duP.: On the Modeling of the Scalar Correlations Necessary to Construct a Second-Order Closure Description of Turbulent Reacting Flows. Turbulent Mixing in Nonreactive and Reactive Flows, S.N.B. Murthy, ed., Plenum Press,(New York) 1975, pp. 131-162.

24. Donaldson, C. duP.; and Varma, A. K.: Remarks on the Construction of a Second-Order Closure Description of Turbulent Reacting Flows, Combustion Science and Technology, Vol. 13, 1976, pp. 55-78.

25. Varma, A. K.; and Donaldson, C. duP.: Development of a Second-Order Closure Model for Computation of Turbulent Diffusion Flames. NASA CR-132524, June 1974.

26. Varma, A. K.; Beddini, R. A.; and Fishburne, E. S.: Second-Order Closure Analysis of Turbulent Reacting Flows. Proceedings of the 1976 Heat Transfer and Fluid Mechanics Institute, 1976.

27. Wygnanski, I.; and Fiedler, H.: Some Measurements in the Self-Preserving Jet, J. Fluid Mech., Vol. 38, pt. 3, September 18, 1969, pp. 577-612.

28. Birch, S. F.; and Eggers, J. M.: Free Turbulent Shear Flows, Vol. I and II, Conference Proceedings, NASA SP-321, 1973.

29. Lewellen, W. S.; Teske, M. E.; and Donaldson, C. duP.: Application of Turbulence Model Equations to Axisymmetric Wakes, AIAA J., Vol. 12, No. 5, 1974, pp. 620-625.

30. Chevray, R.: The Turbulent Wake of a Body of Revolution. Trans. ASME, Ser. D.: J. Basic Eng., Vol. 90, No. 2, June 1968, pp. 275-284.

31. Konrad, J. H.: An Experimental Investigation of Mixing in Two-Dimensional Turbulent Shear Flows with Applications to Diffusion-Limited Chemical Reactions. Ph.D. Thesis, California Institute of Technology, Pasadena, CA, 1976.

32. Beddini, R. A.; Varma, A. K.; and Fishburne, E. S.: A Preliminary Investigation of Velocity-Coupled Erosive Burning, Proceedings of the 13th JANNAF Combustion Meeting, Vol. II, December 1976, pp. 385-406.

33. Pergament, H. S.; and Fishburne, E. S.: Influence of Buoyancy on Turbulent Hydrogen/Air Diffusion Flames. Paper presented at Fluid Mechanics of Combustion Processes Conference, Central States Section, The Combustion Institute, March 28-30, 1977.

TABLE 1. HYDROGEN-AIR REACTION SET

	REACTIONS	$K_F = A*EXP(B/RT)/T**N$ (MOLES-ML-SEC UNITS)		
		A	N	B
1	$H + OH + M = H_2O + M$	.5084E 19	1.0	0.0
2	$H_2O + O = OH + OH$	.5728E 14	0.0	-18800.0
3	$OH + H_2 = H_2O + H$	.2170E 14	0.0	-5200.0
4	$O + H_2 = OH + H$	.1808E 11	-1.0	-8960.0
5	$H + O_2 = OH + O$	.2231E 15	0.0	-16800.0
6	$O + H + M = OH + M$	.7264E 16	0.0	0.0
7	$O + O + M = O_2 + M$	.1379E 19	1.0	-340.0
8	$H + H + M = H_2 + M$	.6535E 18	1.0	0.0

APPENDIX A.

General Conservation Equations for a Turbulent Multicomponent Reacting System

Continuity Equation

$$\rho_t + (\rho u^\ell)_{,\ell} = 0 \tag{1}$$

Momentum Equation

$$\rho u_{j_t} + \rho u^\ell u_{j,\ell} = -p_{,j} + \tau^\ell_{j,\ell} \tag{2}$$

where

$$\tau^\ell_j = g^{\ell k}\mu\left(u_{j,k} + u_{k,j}\right) + \delta^\ell_j \mu^* u^k_{,k} \tag{3}$$

Energy Equation

$$\rho h_t + \rho u^\ell h_{,\ell} - p_t - u^\ell p_{,\ell} = \psi - \sum_\alpha h^o_\alpha \dot{w}_\alpha \tag{4}$$

where

$$h = \sum_\alpha h_\alpha \cdot c_\alpha \tag{5}$$

$$h_\alpha = \int_{T^o}^{T} c_{p_\alpha}\, dT \tag{6}$$

$$\psi = \phi - H \tag{7}$$

$$\phi = \tau^m_\ell u^\ell_{,m} \tag{8}$$

$$H = -g^{\ell m}\left[kT_{,\ell} + \rho \sum h_\alpha D_\alpha c_{\alpha,\ell}\right]_{,m} \tag{9}$$

Species Equation

$$\begin{aligned} \rho c_{\alpha_t} + \rho u^\ell c_{\alpha,\ell} &= \dot{w}_\alpha + g^{\ell m}\left(\rho D_\alpha c_{\alpha,\ell}\right)_{,m} \\ &= \dot{w}_\alpha + G_\alpha \end{aligned} \tag{10}$$

Equation of State

$$p = \rho \mathcal{R} T \sum \frac{c_\alpha}{W_\alpha} \tag{11}$$

In the above-noted equations, the symbols have their usual meaning: $\dot{w}_\alpha$ is the mass rate of formation of component α per unit volume; h^o_α is the heat of formation of species α ; D_α is the diffusion coefficient; and W_α is the species molecular weight.

Writing the dependent variables in these equations as the sum of a mean and a fluctuating part ($u = \bar{u} + u'$; $\rho = \bar{\rho} + \rho'$; etc.), one can derive equations for the mean quantities and the second-order correlations of the fluctuations.

Defining $\bar{\mathcal{D}} f = f_t + \bar{u}^\ell f_{,\ell}$, the equations can be written as

$$\bar{\mathcal{D}}\bar{\rho} + \bar{\rho}\bar{u}^\ell_{,\ell} + \overline{(\rho' u'^\ell)}_{,\ell} = 0 \tag{12}$$

$$\bar{\rho}\bar{\mathcal{D}}\bar{u}_j + \overline{\rho' u'^\ell}\,\bar{u}_{j,\ell} + \overline{(\rho' u'_j)}_t + \left[\bar{\rho}\overline{(u'^\ell u'_j)} + \bar{u}^\ell\overline{(\rho' u'_j)} + \overline{(\rho' u'^\ell u'_j)}\right]_{,\ell} = -\bar{p}_{,j} + \bar{\tau}^\ell_{j,\ell} \tag{13}$$

$$\bar{\rho}\bar{\mathcal{D}}\bar{h} + \overline{\rho' u'^\ell}\,\bar{h}_{,\ell} + \overline{(\rho' h')}_t + \left[\bar{\rho}\overline{(u'^\ell h')} + \bar{u}^\ell\overline{(\rho' h')} + \overline{(\rho' u'^\ell h')}\right]_{,\ell} = \bar{p}_t + \bar{u}^\ell\bar{p}_{,\ell} + \overline{(u'^\ell p'_{,\ell})} + \bar{\psi} - \sum_\alpha h^o_\alpha \bar{\dot{w}}_\alpha \tag{14}$$

$$\bar{\rho}\bar{\mathcal{D}}\bar{c}_\alpha + \overline{(\rho' u'^\ell)}\bar{c}_{\alpha,\ell} + \overline{(\rho' c'_\alpha)}_t + \left[\bar{\rho}\overline{(u'^\ell c'_\alpha)} + \bar{u}^\ell\overline{(\rho' c'_\alpha)} + \overline{(\rho' u'^\ell c'_\alpha)}\right]_{,\ell} = \bar{\dot{w}}_\alpha + \bar{G}_\alpha \tag{15}$$

$$\bar{\rho}\,\bar{\mathcal{D}}(\overline{u_j'u_k'}) + (\overline{\rho' u_j' u_k'})_t + \left[\bar{\rho}(\overline{u'^{\ell} u_j' u_k'}) + \bar{u}^{\ell}(\overline{\rho' u_j' u_k'}) + (\overline{\rho' u'^{\ell} u_j' u_k'})\right]_{,\ell}$$

$$- (\overline{\rho' u'^{\ell}})_{,\ell}(\overline{u_j' u_k'}) + (\overline{\rho' u_k'})\bar{\mathcal{D}}\,\bar{u}_j + (\overline{\rho' u_j'})\bar{\mathcal{D}}\,\bar{u}_k$$

$$+ (\overline{u'^{\ell} u_k'})\bar{\rho}\bar{u}_{j,\ell} + (\overline{u'^{\ell} u_j'})\bar{\rho}\bar{u}_{k,\ell} + (\overline{\rho' u'^{\ell} u_k'})\bar{u}_{j,\ell}$$

$$+ (\overline{\rho' u'^{\ell} u_j'})\bar{u}_{k,\ell}$$

$$= -(\overline{u_k' p'_{,j}}) + (\overline{u_j' p'_{,k}}) + (\overline{u_k' \tau'^{\ell}_{j,\ell}}) + (\overline{u_j' \tau'^{\ell}_{k,\ell}}) \qquad (16)$$

$$\bar{\rho}\,\bar{\mathcal{D}}(\overline{h'h'}) + (\overline{\rho h' h'})_t + \left[\bar{\rho}(\overline{u'^{\ell} h' h'}) + \bar{u}^{\ell}(\overline{\rho' h' h'}) + (\overline{\rho' u'^{\ell} h' h'})\right]_{,\ell}$$

$$- (\overline{\rho' u'^{\ell}})_{,\ell}(\overline{h' h'}) + 2(\overline{\rho' h'})\bar{\mathcal{D}}\,\bar{h} + 2\bar{\rho}\bar{h}_{,\ell}(\overline{u'^{\ell} h'})$$

$$+ 2\bar{h}_{,\ell}(\overline{\rho' u'^{\ell} h'})$$

$$= 2(\overline{h' p_t'}) + 2\bar{u}^{\ell}(\overline{h' p'_{,\ell}}) + 2\bar{p}_{,\ell}(\overline{h' u'^{\ell}}) + 2(\overline{h' u'^{\ell} p'_{,\ell}})$$

$$+ 2(\overline{h'\psi'}) - 2\sum_{\alpha} h_{\alpha}^{o}(\overline{h'\dot{w}_{\alpha}'}) \qquad (17)$$

$$\bar{\rho}\bar{\mathcal{D}}(\overline{u_j'h'}) + (\overline{\rho'u_j'h'})_t + \left[\bar{\rho}(\overline{u'^{\ell}u_j'h'}) + \bar{u}^{\ell}(\overline{\rho'u_j'h'}) + (\overline{\rho'u'^{\ell}u_j'h'})\right]_{,\ell}$$

$$- (\overline{\rho'u'^{\ell}})_{,\ell}(\overline{u_j'h'}) + (\overline{\rho'u_j'})\bar{\mathcal{D}}\bar{h} + (\overline{\rho'h'})\bar{\mathcal{D}}\bar{u}_j$$

$$+ (\overline{u'^{\ell}u_j'})\bar{\rho}\bar{h}_{,\ell} + (\overline{u'^{\ell}h'})\bar{\rho}\bar{u}_{j,\ell} + (\overline{\rho'u'^{\ell}u_j'})\bar{h}_{,\ell}$$

$$+ (\overline{\rho'u'^{\ell}h'})\bar{u}_{j,\ell}$$

$$= (\overline{u_j'p_t'}) + \bar{u}^{\ell}(\overline{u_j'p'_{,\ell}}) + \bar{p}_{,\ell}(\overline{u_j'u'^{\ell}}) + (\overline{u_j'u'^{\ell}p'_{,\ell}}) + (\overline{u_j'\psi'})$$

$$- \sum_{\alpha} h_{\alpha}^{o}(\overline{u_j'\dot{w}_{\alpha}'}) - (\overline{h'\rho'_{,j}}) + (\overline{h'\tau_{j,\ell}'^{\ell}}) \qquad (18)$$

$$\bar{\mathcal{D}}(\overline{\rho'\rho'}) + 2\bar{\rho}_{,\ell}(\overline{\rho'u'^{\ell}}) + 2\bar{u}^{\ell}_{,\ell}(\overline{\rho'\rho'}) + 2\bar{\rho}(\overline{\rho'u_{,\ell}'^{\ell}})$$

$$+ (\overline{\rho'\rho'u_{,\ell}'^{\ell}}) + (\overline{\rho'\rho'u'^{\ell}})_{,\ell} = 0 \qquad (19)$$

$$\bar{\rho}\bar{\mathcal{D}}(\overline{c_{\alpha}'c_{\beta}'}) + (\overline{\rho'c_{\alpha}'c_{\beta}'})_t + \left[\bar{\rho}(\overline{u'^{\ell}c_{\alpha}'c_{\beta}'}) + \bar{u}^{\ell}(\overline{\rho'c_{\alpha}'c_{\beta}'}) + (\overline{\rho'u'^{\ell}c_{\alpha}'c_{\beta}'})\right]_{,\ell}$$

$$- (\overline{\rho'u'^{\ell}})_{,\ell}(\overline{c_{\alpha}'c_{\beta}'}) + (\overline{\rho'c_{\beta}'})\bar{\mathcal{D}}\bar{c}_{\alpha} + (\overline{\rho'c_{\alpha}'})\bar{\mathcal{D}}\bar{c}_{\beta}$$

$$+ (\overline{u'^{\ell}c_{\beta}'})\bar{\rho}\bar{c}_{\alpha,\ell} + (\overline{u'^{\ell}c_{\alpha}'})\bar{\rho}\bar{c}_{\beta,\ell} + (\overline{\rho'u'^{\ell}c_{\beta}'})\bar{c}_{\alpha,\ell}$$

$$+ (\overline{\rho'u'^{\ell}c_{\alpha}'})\bar{c}_{\beta,\ell}$$

$$= (\overline{c_{\beta}'\dot{w}_{\alpha}'}) + \overline{c_{\alpha}'\dot{w}_{\beta}'} + (\overline{c_{\beta}'G_{\alpha}'}) + \overline{c_{\alpha}'G_{\beta}'} \qquad (20)$$

$$\bar{\rho}\bar{\mathcal{D}}(\overline{u_j'c_\alpha'}) + (\overline{\rho'u_j'c_\alpha'})_t + \left[\bar{\rho}(\overline{u'^\ell u_j'c_\alpha'}) + \bar{u}^\ell(\overline{\rho'u_j'c_\alpha'}) + (\overline{\rho'u'^\ell u_j'c_\alpha'})\right]_{,\ell}$$

$$- (\overline{\rho'u'^\ell})_{,\ell}(\overline{u_j'c_\alpha'}) + (\overline{\rho'u_j'})\bar{\mathcal{D}}\bar{c}_\alpha + (\overline{\rho'c_\alpha'})\bar{\mathcal{D}}\bar{u}_j$$

$$+ (\overline{u'^\ell u_j'})\bar{\rho}\bar{c}_{\alpha,\ell} + (\overline{u'^\ell c_\alpha'})\bar{\rho}\bar{u}_{j,\ell} + (\overline{\rho'u'^\ell u_j'})\bar{c}_{\alpha,\ell}$$

$$+ (\overline{\rho'u'^\ell c_\alpha'})\bar{u}_{j,\ell}$$

$$= (\overline{u_j'\dot{w}_\alpha'}) + (\overline{u_j'G_\alpha'}) - (\overline{c_\alpha'p'_{,j}}) + (\overline{c_\alpha'\tau_{j,\ell}'^\ell}) \qquad (21)$$

$$\bar{\rho}\bar{\mathcal{D}}(\overline{h'c_\alpha'}) + (\overline{\rho'h'c_\alpha'})_t + \left[\bar{\rho}(\overline{u'^\ell h'c_\alpha'}) + \bar{u}^\ell(\overline{\rho'h'c_\alpha'}) + (\overline{\rho'u'^\ell h'c_\alpha'})\right]_{,\ell}$$

$$- (\overline{\rho'u'^\ell})_{,\ell}(\overline{h'c_\alpha'}) + (\overline{\rho'h'})\bar{\mathcal{D}}\bar{c}_\alpha + (\overline{\rho'c_\alpha'})\bar{\mathcal{D}}\bar{h}$$

$$+ (\overline{u'^\ell h'})\bar{\rho}\bar{c}_{\alpha,\ell} + (\overline{u'^\ell c_\alpha'})\bar{\rho}\bar{h}_{,\ell} + (\overline{\rho'u'^\ell h'})\bar{c}_{\alpha,\ell}$$

$$+ (\overline{\rho'u'^\ell c_\alpha'})\bar{h}_{,\ell}$$

$$= (\overline{h'\dot{w}_\alpha'}) + (\overline{h'G_\alpha'}) + (\overline{c_\alpha'p_t'}) + \bar{u}^\ell(\overline{c_\alpha'p'_{,\ell}}) + \bar{p}_{,\ell}(\overline{c_\alpha'u'^\ell})$$

$$+ (\overline{c_\alpha'u'^\ell p'_{,\ell}}) + (\overline{c_\alpha'\psi'}) - \sum_\beta h_\beta^o(\overline{\dot{w}_\beta'c_\alpha'}) \qquad (22)$$

$$\bar{\rho}\mathcal{D}(\overline{\rho' u_j'}) + (\overline{\rho'\rho' u_j'})_t + \left[\bar{\rho}(\overline{u'^{\ell}\rho' u_j'}) + \bar{u}^{\ell}(\overline{\rho'\rho' u_j'}) + (\overline{\rho'\rho' u'^{\ell} u_j'})\right]_{,\ell}$$

$$- (\overline{\rho' u'^{\ell}})_{,\ell}(\overline{\rho' u_j'}) + (\overline{\rho'\rho'})\mathcal{D}\bar{u}_j + (\overline{\rho' u_j'})\mathcal{D}\bar{\rho}$$

$$+ (\overline{u'^{\ell}\rho'})\bar{\rho}\bar{u}_{j,\ell} + (\overline{u'^{\ell} u_j'})\bar{\rho}\bar{\rho}_{,\ell} + (\overline{\rho'\rho' u'^{\ell}})\bar{u}_{j,\ell}$$

$$+ (\overline{\rho' u_j' u'^{\ell}})\bar{\rho}_{,\ell}$$

$$= -(\overline{\rho' p'_{,j}}) + (\overline{\rho' \tau'^{\ell}_{j,\ell}}) - \left[\bar{\rho}\bar{\rho}(\overline{u'^{\ell}_{,\ell} u_j'}) + 2\bar{\rho}\bar{u}^{\ell}_{,\ell}(\overline{\rho' u_j'})\right.$$

$$\left. + 2\bar{\rho}(\overline{\rho' u'^{\ell}_{,\ell} u_j'}) + \bar{u}^{\ell}_{,\ell}(\overline{\rho'\rho' u_j'}) + (\overline{\rho'\rho' u'^{\ell}_{,\ell} u_j'})\right] \tag{23}$$

$$\bar{\rho}\mathcal{D}(\overline{\rho' h'}) + (\overline{\rho'\rho' h'})_t + \left[\bar{\rho}(\overline{u'^{\ell}\rho' h'}) + \bar{u}^{\ell}(\overline{\rho'\rho' h'}) + (\overline{\rho'\rho' u'^{\ell} h'})\right]_{,\ell}$$

$$- (\overline{\rho' u'^{\ell}})_{,\ell}(\overline{\rho' h'}) + (\overline{\rho'\rho'})\mathcal{D}\bar{h} + (\overline{\rho' h'})\mathcal{D}\bar{\rho}$$

$$+ (\overline{u'^{\ell}\rho'})\bar{\rho}\bar{h}_{,\ell} + (\overline{u'^{\ell} h'})\bar{\rho}\bar{\rho}_{,\ell} + (\overline{\rho'\rho' u'^{\ell}})\bar{h}_{,\ell} + (\overline{\rho' h' u'^{\ell}})\bar{\rho}_{,\ell}$$

$$= + (\overline{\rho' p'_t}) + \bar{u}^{\ell}(\overline{\rho' p'_{,\ell}}) + \bar{p}_{,\ell}(\overline{\rho' u'^{\ell}}) + (\overline{\rho' u'^{\ell} p'_{,\ell}})$$

$$+ (\overline{\rho'\psi'}) - \sum_{\alpha} h^{o}_{\alpha}(\overline{\rho' \dot{w}'_{\alpha}}) - \left[\bar{\rho}\bar{\rho}(\overline{u'^{\ell}_{,\ell} h'}) + 2\bar{\rho}\bar{u}^{\ell}_{,\ell}(\overline{\rho' h'})\right.$$

$$\left. + 2\bar{\rho}(\overline{\rho' h' u'^{\ell}_{,\ell}}) + \bar{u}^{\ell}_{,\ell}(\overline{\rho'\rho' h'}) + (\overline{\rho'\rho' h' u'^{\ell}_{,\ell}})\right] \tag{24}$$

$$\bar{\rho}\bar{\mathcal{D}}(\overline{\rho' c_\alpha'}) + (\overline{\rho'\rho' c_\alpha'})_t + \left[\bar{\rho}(\overline{u'^{\ell}\rho' c_\alpha'}) + \bar{u}^{\ell}(\overline{\rho'\rho' c_\alpha'}) + (\overline{\rho'\rho' u'^{\ell} c_\alpha'})\right]_{,\ell}$$

$$- (\overline{\rho' u'^{\ell}})_{,\ell}(\overline{\rho' c_\alpha'}) + (\overline{\rho'\rho'})\bar{\mathcal{D}}\,\bar{c}_\alpha + (\overline{\rho' c_\alpha'})\bar{\mathcal{D}}\,\bar{\rho}$$

$$+ (\overline{u'^{\ell}\rho'})\bar{\rho}\bar{c}_{\alpha,\ell} + (\overline{u'^{\ell} c_\alpha'})\bar{\rho}\bar{\rho}_{,\ell} + (\overline{\rho'\rho' u'^{\ell}})\bar{c}_{\alpha,\ell} + (\overline{\rho' c_\alpha' u'^{\ell}})\bar{\rho}_{,\ell}$$

$$= +(\overline{\rho' \dot{w}_\alpha'}) + (\overline{\rho' G_\alpha'}) - \left[\bar{\rho}\bar{\rho}(\overline{u'^{\ell}_{,\ell} c_\alpha'}) + 2\bar{\rho}\bar{u}^{\ell}_{,\ell}(\overline{\rho' c_\alpha'})\right.$$

$$\left. + 2\bar{\rho}(\overline{\rho' c_\alpha' u'^{\ell}_{,\ell}}) + \bar{u}^{\ell}_{,\ell}(\overline{\rho'\rho' c_\alpha'}) + (\overline{\rho'\rho' c_\alpha' u'^{\ell}_{,\ell}})\right] \tag{25}$$

Detailed expressions for terms like $\bar{\psi}$, ψ' , $\bar{G}_\alpha$, G_α' , etc. can be obtained from their definitions. The expressions for the reaction source terms $\bar{\dot{w}}_\alpha$ and $\dot{w}_\alpha'$ will be obtained from the modeling of the chemical reaction. As an example, if one uses a one-step chemical reaction model

$$\sum_{\alpha=1}^{N} \nu_\alpha' M_\alpha \rightarrow \sum_{\alpha=1}^{N} \nu_\alpha'' M_\alpha \tag{26}$$

the reaction rate term can be written as

$$\dot{w}_\alpha = W_\alpha(\nu_\alpha'' - \nu_\alpha') \, A T^n \exp\left(-\frac{E}{\mathcal{R}T}\right) \prod_{\alpha=1}^{N} \left(\frac{\rho c_\alpha}{W_\alpha}\right)^{\nu_\alpha'} \tag{27}$$

Expressions for $\bar{\dot{w}}_\alpha$ and $\dot{w}_\alpha'$ can be obtained.

APPENDIX B.

Limiting Value of the Unmixedness Correlation for a Simple Reacting Flow

Consider a constant temperature, constant density, reacting flowfield of two species α and β that react according to the simple one-step reaction $\alpha + \beta \xrightarrow{k} \gamma$. The unmixedness correlation for this case is $\frac{\overline{\alpha'\beta'}}{\bar{\alpha}\bar{\beta}}$. A limiting value for this correlation can be derived for large, but finite k.

The conservation equations for $\bar{\alpha}$, $\bar{\beta}$ and $\overline{\alpha'\beta'}$ for this case are:

$$\frac{D\bar{\alpha}}{Dt} = \frac{\nu}{Sc}\frac{\partial^2\bar{\alpha}}{\partial y^2} - \frac{\partial}{\partial y}\overline{v'\alpha'} - k_\alpha(\bar{\alpha}\bar{\beta} + \overline{\alpha'\beta'}) \tag{1}$$

$$\frac{D\bar{\beta}}{Dt} = \frac{\nu}{Sc}\frac{\partial^2\bar{\beta}}{\partial y^2} - \frac{\partial}{\partial y}\overline{v'\beta'} - k_\beta(\bar{\alpha}\bar{\beta} + \overline{\alpha'\beta'}) \tag{2}$$

$$\begin{aligned}\frac{D\overline{\alpha'\beta'}}{Dt} = &- \overline{v'\alpha'}\frac{\partial\bar{\beta}}{\partial y} - \overline{v'\beta'}\frac{\partial\bar{\alpha}}{\partial y} - \frac{\partial}{\partial y}(\overline{v'\alpha'\beta'}) \\ &+ \frac{\nu}{Sc}\frac{\partial^2}{\partial y^2}\overline{\alpha'\beta'} - 2\frac{\nu}{Sc}\frac{\overline{\alpha'\beta'}}{\lambda^2} \\ &- k_\alpha(\bar{\alpha}\,\overline{\beta'\beta'} + \bar{\beta}\,\overline{\alpha'\beta'} + \overline{\alpha'\beta'\beta'}) \\ &- k_\beta(\bar{\alpha}\,\overline{\alpha'\beta'} + \bar{\beta}\,\overline{\alpha'\alpha'} + \overline{\alpha'\alpha'\beta'})\end{aligned} \tag{3}$$

where $k_\alpha = \frac{\rho k}{W_\beta}$, $k_\beta = \frac{\rho k}{W_\alpha}$

Multiplying Eq. (1) by $\bar{\beta}$, Eq. (2) by $\bar{\alpha}$ and adding the resulting equations to Eq. (3) one can obtain:

$$\begin{aligned}\frac{D}{Dt}(\bar{\alpha}\bar{\beta} + \overline{\alpha'\beta'}) = &\frac{\nu}{Sc}\left(\bar{\beta}\frac{\partial^2\bar{\alpha}}{\partial y^2} + \bar{\alpha}\frac{\partial^2\bar{\beta}}{\partial y^2} + \frac{\partial^2}{\partial y^2}\overline{\alpha'\beta'}\right) \\ &- \frac{\partial}{\partial y}(\bar{\alpha}\,\overline{v'\beta'} + \bar{\beta}\,\overline{v'\alpha'} + \overline{v'\alpha'\beta'}) \\ &- k_\alpha(\bar{\alpha}\,\overline{\beta'\beta'} + \bar{\beta}\,\overline{\alpha'\beta'} + \overline{\alpha'\beta'\beta'})\end{aligned}$$

$$- k_\beta(\bar{\alpha}\ \overline{\alpha'\beta'} + \bar{\beta}\ \overline{\alpha'\alpha'} + \overline{\alpha'\alpha'\beta'})$$

$$- 2\frac{\nu}{Sc}\frac{\overline{\alpha'\beta'}}{\lambda^2} - (k_\alpha\bar{\beta} + k_\beta\bar{\alpha})(\bar{\alpha}\bar{\beta} + \overline{\alpha'\beta'})$$

Consider the case of high Reynolds number $(\nu \to 0)$

$$\lambda^2 \cong \frac{bq}{\Lambda\nu}$$

$$\frac{D}{Dt}(\bar{\alpha}\bar{\beta} + \overline{\alpha'\beta'}) = -\frac{\partial}{\partial y}(\bar{\alpha}\ \overline{v'\beta'} + \bar{\beta}\ \overline{v'\alpha'} + \overline{v'\alpha'\beta'})$$

$$- k_\alpha(\bar{\alpha}\ \overline{\beta'\beta'} + \bar{\beta}\ \overline{\alpha'\beta'} + \overline{\alpha'\beta'\beta'})$$

$$- k_\beta(\bar{\alpha}\ \overline{\alpha'\beta'} + \bar{\beta}\ \overline{\alpha'\alpha'} + \overline{\alpha'\alpha'\beta'})$$

$$- \frac{2b}{Sc} \cdot \frac{q}{\Lambda} \cdot \overline{\alpha'\beta'} - (k_\alpha\bar{\beta} + k_\beta\bar{\alpha})(\bar{\alpha}\bar{\beta} + \overline{\alpha'\beta'}) \quad (4)$$

For fast chemistry, $\alpha\beta \to 0$, consider $\alpha\beta = \varepsilon$, ε small

$$\bar{\alpha}\bar{\beta} + \overline{\alpha'\beta'} = \bar{\varepsilon} \quad (5)$$

$$\bar{\alpha}\beta' + \bar{\beta}\alpha' + \overline{\alpha'\beta'} - \overline{\alpha'\beta'} = \varepsilon' \approx 0 \quad (6)$$

using Eq. (6) in Eq. (4)

$$\frac{D}{Dt}(\bar{\alpha}\bar{\beta} + \overline{\alpha'\beta'}) = -\frac{2b}{Sc} \cdot \frac{q}{\Lambda} \cdot \overline{\alpha'\beta'}$$

$$- (k_\alpha\bar{\beta} + k_\beta\bar{\alpha})(\bar{\alpha}\bar{\beta} + \overline{\alpha'\beta'}) \quad (7)$$

The asymptotic limit for the term $(\bar{\alpha}\bar{\beta} + \overline{\alpha'\beta'})$ can be obtained by neglecting the convective term in Eq. (7).

$$\bar{\alpha}\bar{\beta} + \overline{\alpha'\beta'} \simeq \frac{-\frac{2b}{Sc} \cdot \frac{q}{\Lambda}\overline{\alpha'\beta'}}{(k_\alpha\bar{\beta} + k_\beta\bar{\alpha})}$$

$$\simeq \frac{+\frac{2b}{Sc}\cdot\frac{q}{\Lambda}\,\bar{\alpha}\bar{\beta}}{(k_\alpha\bar{\beta} + k_\beta\bar{\alpha})} \qquad (8)$$

Eq. (8) gives the limiting value of $\frac{\overline{\alpha'\beta'}}{\bar{\alpha}\bar{\beta}}$ for fast chemistry and high Reynolds number.

APPENDIX C

The input cards for a multi-step chemistry reacting shear layer (RSL) run are listed below:

Card 1	INFLG, XINPT, LSWTCH, TIMXI	(I1, 7X, E8.0 4X, 16L1, 36X, 2F4.0)
Card 2	NRUNI, SERID, CMNTS	(I4, 19A4)
Card 3	MSTEP, MBKUP, JMAX, MXPAN, MRST, NRLMN NSKAA, NDCAA, NAALS	(2I4, 32X, 10I4)
Card 4	NIOLP, NIOPP, NFOLP, NFOPP	(20I4)
Card 5	TBRKV(I),(I=1, MTBRK)	(10E8.0)
Card 6	DXINP, DXMIN, DXMAX, DXFMX, BUFAC, CRTRN, PCTLV, PCTHV, EPTSC	(10E8.0)
Card 7	EPNUS, EPNTS, EPNCS, EPNUU, EPNUT, EPNTT, EPNUC, EPNTC, EPNCC	(10E8.0)
Card 8	EPBUS, EPBTS, EPBCS, EPBUU, EPBUT, EPBTT, EPBUC, EPBTC, EPBCC	(10E8.0)
Card 9	EPTUS, EPTTS, EPTCS, EPTUU, EPTUT, EPTTT, EPTUC, EPTTC, EPTCC	(10E8.0)
Card 10	YMIN, YMAX, ECMNI, ECMXI, FCURI, FCMX, DYFMN, DYFMX, DYRMX	(10E8.0)
Card 11	NFLTP, ICTYP, NSPCI, NVBCN, NTPLS, N2OCL, N3OCL, LAMNF, LINCF, LCMPF, LSPCF, LSP01, LYLFF, LYHFF, LP0WL, LINRT, LNUPW, LORIG, LAXSM, LPHPT, LNFTS, LENCF, LPRLV	(7I4, T41, 40L1)
Card 12	ASL, BSL, BETSL, ABL, BBL, CBL, FDIVU, WMD, VMRD	(10E8.0)
Card 13	VMXYV(I),(I=1, NCVTM)	(10E8.0)
Card 14	FSXYV(I),(I=1,NCVTM)	(10E8.0)
Card 15	WMU, WMR, WMH, WMT, WMC, WWGU, WWGR, WWGH, WWGT, WWGC	(10E8.0)

Card 16	WMWU1, WMWR1, WMWH1, WMWT1, WMWC1	(10E8.0)
Card 17	WMWU2, WMWR2, WMWH2, WMWT2, WMWC2	(10E8.0)
Card 18	WGU1, WGR1, WGH1, WGT1, WGC1, WGU2, WGR2, WGH2, WGT2, WGC2, WGU3, WGR3, WGH3, WGT3, WGC3	(10E8.0)
Card 19	PMU, PMR, PMH, PMC, PMU2, PMR2, PMH2, PMC2	(10E8.0)
Card 20	PGU, PGR, PGH, PGC, PGU2, PGR2, PGH2, PGC2	(10E8.0)
Card 21	PTMU, PTMR, PTMH, PTMC	(10E8.0)
Card 22	UREF, REFL, TREF, PREF, UGASC, VBNDC, DPDX, RADX	(10E8.0)
Card 23.n	SPCNV(1,I), SPCNV(2,I), CREF(I), CSECI(I), WMOLN(I), HOSC(I), TOSC(I)	(2A4, 5E8.0)
Card 24.n	CPSCO(IC, I), IC=2, MCPCO	(5E16.0)
Card 25.n	EMUCO(IC,I), IC=1,2, MESCO(IC,I), IC=1,2 CAYCO(IC,I), IC=1,2, DIFCO(IC,I), IC=1,2	(10E8.0)
Card 26	FWRCO	(10E8.0)
Card 27	KSTCO(I,IC), STOCO,(I,IC), I=1, NSPEC, IC=1,2	(40(A1, E7.0))
Card 28	ACEF, AWMLE, ASTCK	(10E8.0)
Card 29	ABXHO	(10E8.0)
Card 30	NBXMD, LBXGO, LBXPR, LBXPC, LAKTB, LAKAB, LAKCC, LBXMI, LBXIN, LSFLA, LBXCO, LACXO, LSFCC, LSFPC	(I4, T41, 40L1)
Card 31	KPVNB(1), KPVTB(I), I=1, NFLDS	(10(A4, 1X, A1, 2X)
Card 32	PREML(I), I=1, NPRVI	(10E8.0)
Card 33	PREAD(I), I=1, NPRVI	(10E8.0)
Card 34	YVZ(I), I=1, NPRVI	(10E8.0)
Card 35	IKINE, NGAM, NALP, NBET, NTURBC, MDIAG, MVC, MCPCO, NSE, NHMAX, MKBAR, MTPAP	(2014)

Card 36	DELC, DELH, TKINET, TOLER, ALMIN, BEMIN	(8E10.0)
Card 37	UNMIX, XFACT, CCFACT	(8E10.0)
Card 38	AID(I), MW(I)	(A4,E10.0)
Card 39	EMU(I), EOMEGA(I), EMS(I), ESEGA(I), CAX(I), CSEGA(I), DIF(I), DIEGA(I)	((7E10.0,E6.0)
Card 40	A(1), A(2), A(3), A(4)	(4E13.5)
Card 41	A(5), A(6)	(3E13.5)
Card 42	FA(1)	(8E10.0)
Card 43	FA(2)	(8E10.0)
Card 44	FA(3)	(8E10.0)
Card 45	IZD(1), IZD(2), IZD(3), IZD(4), IZD(5), IRR, IRT, RC(1), RC(2), RC(3)	(A4, 3X, A4, 10X, A4, 3X, A4, 9X, I2, I1, E8.2, F4.1, F9.1)

A card-by-card description of the input deck follows. Default values or recommended values are in parentheses.

Card 1

INFLG — 0 restart of current job
1 flags a new run and all the cards are read.
2 restart of job with changes.
(This feature is under development and is not operational at present.)

XINPT — Value of x at the initial profile station. Used only for a new run.

LSWTCH — Normally all false(F). Sequence of switches numbered 0-15 used to activate various output/diagnostic output options. For example,
SW1 True (T) minor output every step
SW2 True (T) full printout every step, etc.

TIMXI — Run time in decimal minutes. If time on the job card is smaller, it overrides TIMXI.

Card 2

NRUNI — User labelled run number. If zero, will increment last run number.

SERID — Four-character run series identification.

CMNTS — Comments on run to be printed on the title page - up to 76 characters.

Card 3

MSTEP — Maximum number of steps allowed (2000).

MBKUP — Number of backups allowed. If number of backups exceed MBKUP, the run exits with error message (6).

JMAX — Maximum number of points allowed across the profile (default value is JMXMX specified in RSLIN).

MXPAN — Maximum number of points that can be added for an asymptotic boundary condition in one step. Warning message is printed if MXPAN points are added (4).

MRST — Is the first record number when loading an initial profile with an asymptotic lower boundary condition. The empty records below MRST may be used for profile expansion on the first step. Note MRST > MEXPAN.

NRLMN — If flow has a lower asymptotic boundary condition, NRLMN is the record number at which attempted profile recentering by RSLAA will occur automatically. On input NRLMN > MRST > MXPAN for asymptotic lower boundary conditions.

NSKAA — The RSLAA subroutine for adjusting the spacing of points in the y direction is skipped for the first NSKAA steps after startup.

NDCAA — Mandatory call to RSLAA every NDCAA steps. (1).

NAALS — Index for flow length scale to be used in normalizing curvature requirements for RSLAA.
= 1 for absolute y spread
= 2 for TYPL

Card 4

NIOLP — Steps between minor printouts at line printer.

NIOPP — Steps between calls to RSLRF for intermediate plot run-file. RSLRF must be user installed.

NFOLP — Steps between full printouts at line printer.

NFOPP — Steps between calls to RSLPF for full profile output to a plot file. RSLPF must be user installed.

Card 5

TBRKV — Time break vector. Full printouts are forced for values of x (or time) equal to the elements of TBRKV. Up to 20 values may be input on two cards. If the 10th value is in monotonic sequence then a second card is required. The run is halted when a non-monotonic element (e.g., 0) is encountered.

Card 6

DXINP — Initial input value of step size in the x direction, Δx .

DXMIN — Minimum Δx allowed (10^{-8}) .

DXMAX — Maximum Δx allowed. If specified as a negative number, the maximum Δx = number x local macroscale Λ (-0.5).

DXFMX — Maximum ratio by which Δx may increase from one step to the next (4.5).

BUFAC — Maximum ratio by which EPT--criteria may be exceeded without causing a backup (2 or 3).

CRTRN — Variables subject to CRTRN control are set zero if calculated values are lower. (0).

PCTLV — Percent low value of normalized profile used for Λ scale calculation

PCTHV — Percent high value

typical values for		PCTLV	PCTHV
$\bar{u}$ profile	shear layer	0.25	0.75
	axisymmetric jet	0.50	1.00
q^2 profile	shear layer	0.25	1.00
	axisymmetric jet	0.25	not used

EPTSC — A warning is printed if the relative change in the typical length scale in one step, (ΔTYPL/TYPL) is greater than EPTSC.

Card 7

EPN-- — When the absolute value of a variable is less than the absolute value of EPN--, the corresponding variable is not checked in the determination of Δx , nor in considering where to insert or drop points, nor in checking the outer boundary conditions if EPB-- is

negative. Further, if EPN-- is negative, the change in the corresponding variable is compared with the larger of - EPN-- and the criterion derived from EPS-- .

Card 8

EPB-- The solution is extended in the normal direction until the difference between the calculated value of each variable and its asymptotic value is less than EPB-- or -EPB-- * maximum value of the variable, whichever is positive.

Card 9

EPT-- Δx is controlled by attempting to keep the change in each variable in the axial direction below EPT-- or -EPT-- * maximum value of the variable, whichever is positive. This is true for the critical variables as controlled by EPN-- .

Card 10

YMIN
YMAX — minimum and maximum values of y to which the solution may spread. Calculations are not terminated on encountering these but further results are generally not useful.

ECMNI — Curvature tolerances

ECMXI — Govern dropping and adding of points to the profile (.02, .05).

FCURI — Factor by which ECMNI and ECMXI are increased when JMAX impedes the addition of points to the profile (1.1).

FCMX — Maximum factor by which ECMNI and ECMXI may be increased through repeated use of FCURI (5).

DYFMN — Minimum Δy is DYFMN * TYPL. TYPL is calculated with the use of PCTLV and PCTHV. (0).

DYFMX — Maximum Δy is DYFMX * TYPL (.15).

CYRMX — Maximum ratio of two adjacent values of Δy .

Card 11

NFLTP — Flow type index
1 boundary layer
2 wall jet (not checked out)

3 mixing layer
4 jet cascade
5 jet/wake

ICTYP — Type of initial conditions
1 profile input by cards
2 canned cosine profile (only valid for shear layers (flow type 2) at this time.

NSPCI — Number of species groups (3).

NVBCN — Boundary condition on $\bar{v}$.

-1	$\bar{v} = 0$	at	YMIN
0	$\bar{v} = 0$	at	Y = 0
+1	$\bar{v} = 0$	at	YMAX
2	$\bar{v} \equiv 0$	at	all Y

If VBNDC is specified on card 22, the zeroes are replaced by VBNDC.

NTPLS — Type of length scale, TYPL calculation
1 length scale based on $\bar{u}$
2 length scale based on q^2
3 length scale based on total Y spread = YMAX - YMIN
4 TYPL = centerline to PCTLV of $\bar{u}$ profile
5 TYPL = centerline to PCTLV of q^2 profile

N2OCL — Type of closure for scalar correlations

N3OCL
1 simplified typical eddy model.
2 secondary model

Logical Flags

	column	Optimized runs (normally set False (F) set True (T) for desired options)
LAMNF	41	Restrict to passes for laminar computations
LINCF		Restrict to passes for constant density temperature incompressible turbulent flows
LCMPF		Restrict to passes for single species compressible flows
LSPCF		Multi-species, compressible, turbulent flow last 3 flags are mutually exclusive
LSP01		Insure $0 \leq \bar{\alpha} \leq 1$ in computing reaction rate expression
LYLFF	46	Fixed lower boundary flow.
LYHFF		Fixed upper boundary flow.

LPOWL		If true T, power law is used for the temperature dependence of μ , μ^* , k etc. If false F, Sutherland law is used.
LINRT		$\dot{w}$ routine not called. Used for nonreacting flow
LNUPW		Inhibit upwind differencing
LORIG	51	not operational
LAXSM		True for axisymmetric flow
LPHPT		Phantom point procedure used for lower fixed boundary jet flows
LNFTS		$\bar{\bar{T}}$ calculation neglects effect of fluctuations
LWLSL		For boundary layer flows (flow type 1), the value of the temperature slope at the wall will be calculated using the first two points of the initial profile and this value will be maintained throughout the run.

A.R.A.P. Turbulence Model Parameters

Card 12

ASL	a = 3.25
BSL	b = 0.125
BETSL	$\beta = \begin{cases} 0 \text{ for isotropic dissipation} \\ 1 \text{ for anisotropic dissipation} \end{cases}$
ABL BBL CBL	boundary layer scale Λ Λ = ABL + BBL * Y ABL = 0 Λ = CBL * TYPL BBL = 0.65

0.5	$\bar{u}$ based scale for shear layer and axisymmetric jet
0.6	q^2 scale for shear layer
0.2	q^2 scale for axisymmetric jet.

Note: for boundary 0.17 layer flows $\delta_{.99}$ for boundary layer flows.
Λ = minm of ((ABL + BBL * y) , (0.17 * δ_{99}))

FDIVU

WMD — not used at present.

VMRD

Card 13 (2 cards)

VMXYV — Velocity diffusion coefficient
usually $\begin{cases} 0.1 \text{ if WMW-1} = -0.1 \\ 0.3 \text{ if WMW-1} = +0.3 \end{cases}$
changed if $\Lambda_{scalar} \neq \Lambda_{\bar{u}}$

Card 14 (2 cards)

FSXYV — Turbulence microscale λ factors
1.0 for velocity correlations
1.8 for correlations involving scalars
usually changed if $\Lambda_{scalar} \neq \Lambda_{\bar{u}}$

Card 15

WM-
WWG- — Pressure correlation model parameters

Card 16

WMW=1 — Pressure correlation model parameters

Card 17

WMW-2 — Pressure correlation model parameters

Card 18 (2 cards)

WG-1
WG-2
WG-3 — Pressure correlation model parameters

Card 19

PM-
PM-2 — Pressure correlation model parameters

Card 20

PG-
PG-2 — Pressure correlation model parameters

Card 21

PTM- — Pressure correlation model parameters

End of turbulence model parameters

Card 22

UREF	Reference stream velocity in m/sec
REFL	Reference length in meters
TREF	Reference stream temperature °K
PREF	Reference pressure newtons/m^2
UGASC	Universal gas constant joules/kgmole °K (8314.3)
VBNDC	Additive constant for the $\bar{v}$ profile
DPDX	Axial pressure gradient (not operational)
RADX	Radius of point closest to the centerline of axisymmetric flowfield for nonphantom point calculation procedure.

Set of three cards is required for each chemical species. Program has only been run with n = 3 species cards up to now.

Card 23.n

SPCNV	Chemical species name or symbol.
CREF	Mass concentration in reference stream
CSECI	Mass concentration in secondary stream
WMOLN	Molecular weight
HOSC	Heat of formation at temperature TOSC Kcal/Kgmole
TOSC	Reference temperature for HOSC

Card 24.n

CPSCO Polynomial coefficients for specific heat calculation

$$\frac{C_p}{R} = a_2 + a_3 T + a_4 T^2 + a_5 T^3 + a_6 T^4$$

Card 25.n

EMUCO(1)	μ	at reference temperature
EMSCO(1)	μ^*	
CAYCO(1)	k	
DIFCO(1)	D	

EMUCO(2)
EMSCO(2)
CAYCO(2)
DIFCO(2)

respective exponents for temperature dependence of molecular transport properties

Card 26

FWRCO — Reaction rate coefficients A, N, E_A with,

$$k = AT^N \exp\left(-\frac{E_A}{RT}\right)$$

Card 27

KSTCO — Symbolic characters used for printing reaction, e.g., (+ , =)

STOCO — Stoichometric coefficients used in reaction expression.

Card 28

ACEF — Proportion of actual reactant in species mixtures.

AWMLE — Molecular weights of actual reactants in species mixtures.

ASTCK — Effective stoichometry of reactants used in empirical reaction rate specifications.

Card 29

ABXHO — Not used at present. Was used in connection with alternate "typical eddy" models.

Card 30 — (Logical Flags normally F. Set T for desired options)

NBXMD — "typical eddy" model version 1 , simplified model.

LBXGO — Not used at present.

LBXPR — Prints details of "typical eddy" operation following full printouts.

LBXPC — Prints constrained values of inputs to the "typical eddy" model.

Options for chemical source term $\dot{\bar{w}}$

LAKTB — $\bar{k}$ is calculated from $\bar{T}$ only for chemical source term

	column	
LAKAB	45	$\bar{\dot{w}} = \bar{k}\bar{\alpha}\bar{\beta}$ only, "laminar chemistry"
LAKCC		$\bar{\dot{w}} = \bar{k}(\bar{\alpha}\bar{\beta} + \bar{\alpha}'\bar{\beta}')$ "turbulent chemistry" neglecting k' terms
End options for chemical source terms		
LBXMI		Statistical constraints are used to modify program computations
LBXIN		Inhibits "typical eddy" model operation to single cell. Automatically set true if N20CL = N30CL = 2 in card 11.
LSFLA		Single step reaction RSL program is linked to multi-step chemistry procedure.
LBXCO		"typical eddy" model constraints are only applied to separately printed variables CS, CC etc. when LBXPC is on.
LACXO		Species correlations passes are skipped $\bar{\alpha}'\bar{\phi}' \equiv 0$.
LSFCC		Conservation constraints are used to modify program computations
LSFPC		Conservation constrained output is printed subsequent to a normal printout.
Initial profile input from cards		
Card 31.n		
KPVNB		The left justified names of the independent variable Y and the dependent variables for which nonzero initial profiles are specified. The complete list of names of the variables that can be used are shown in a typical RSL output. For example, US, TS or HS, CS1, CS2, CS3, UU, UV, etc. The first blank name terminates the KPVNB vector.
KPVTB		Not used at present.
Card 32.n		
PREML		Premultiplers for the named input values of initial profile variables.

Card 33.n

PREAD — Additive term for initial profile data after use of premultiplier

Card 34.i

YVZ — Initial profile data set completion is signaled by a nonmonotonic Y value

Note: If UU is specified as a negative value in the initial profile, UU, VV and WW are set equal to the magnitude of UU at the initial station.

The following cards are read only for a calculation which links to the multi-step chemistry package by setting the logical flag LSFLA in column 49 on card 30. For these runs the reaction rate parameters on card 26 must be set zero as the elementary reactions and their rates are specified in detail on cards 48.n.

Card 35

IKINE — Number of elementary reactions

NGAM — Number of chemical species in mixture γ

NALP — Number of chemical species in mixture α

NBET — Number of chemical species in mixture β

NTURBC — 0 for "laminar chemistry." Scalar correlations are neglected in the chemical source terms.

1 for "turbulent chemistry." $\bar{k} = k(\bar{T})$ and all correlations except those involving k' are used in the chemical source terms

MDIAG — 1 diagnostic output for specific heat, enthalpy and entropy parameters.
0 normal program mode. No diagnostic output.

MVC — 1 normal value. $\overline{v'\alpha'}$ transport is included in the species diffusion computations
0 $\overline{v'\alpha'}$ terms are neglected.

MCPCO — Number of polynomial coefficients in specific heat calculation. 5 is the normal value. 2 for C_p independent of temperature.

NSE — 1 superequilibrium subroutine used to calculate the species correlations
0 superequilibrium procedure not used.

NHMAX
- 1 enthalpy change computed relative to the global maximum of enthalpy
- 0 enthalpy change computed relative to the local value of the enthalpy

MKBAR
- 1 mean reaction rate $\bar{k}$ is calculated including second-order correlations
- 0 $\bar{k} = k(\bar{T})$

MTPAP
- 1 k' terms are included in reaction source term
- 0 k' terms are neglected

Card 36

DELC — Maximum species change allowed per step

DELH — Maximum percentage enthalpy change allowed per step

TKINET — Chemical kinetic calculations are skipped for $T < TKINET$. If input value is 0, TKINET = 400°K.

TOLER — If mean species mode fractions are smaller than TOLER, the unmixedness correlations $\overline{\alpha'\beta'}/\bar{\alpha}\bar{\beta}$, etc. are not used in the reaction source term correction factors. FALBE etc. are set zero.

ALMIN — Species α values below WLMIN are set zero

BEMIN — Species β values below BEMIN are set zero

Card 37

UNMIX — Unmixedness limit value. If FALBE etc. are smaller than UNMIX, they are set equal to it.

XFACT — For $X < XFACT$, the superequilibrium values of species correlations are reduced by the factor X/XFACT. Enables gradual buildup of the species correlations.

CCFACT — Multiplier factor for species correlations
- $> 0.$ mulitplier SCMOD is CCFACT
- $= 0.$ multiplier SCMOD is X/XFACT
- $< 0.$ multiplier SCMOD is RRM/RR

RRM is $\overline{\rho'\rho'}$ calculated in RSL
RR is $\overline{\rho'\rho'}$ calculated using superequilibrium

The next group of cards are the chemical species cards. There are four cards per species. Separate card sets have to be input for the species that compose the mixture γ, the mixture α, and the mixture β respectively.

Card n. 38

AID — Species identification

MW — Molecular weight

Card n. 39

EMU — Viscosity μ at reference temperature gm/cm sec

EMS — Second coefficient of viscosity μ^* at reference temperature (0.).

CAY — Prandtl number at reference temperature. It is used to calculate the thermal conductivity k at the reference temperature.

DIF — Schmidt number at reference temperature. It is used to calculate the diffusion coefficient D at the reference temperature.

EOMEGA — ω_μ exponents in polynomials

ESEGA — ω_{μ^*} for temperature dependence

CSEGA — ω_k of molecular transport

DIEGA — ω_D properties. For example $\tilde{\mu} \sim \mathring{\omega}_\mu$

Card n. 40

A(1)
A(2)
A(3)
A(4) — Specific heat polynomial constants

Card n. 41

A(5) — Specific heat polynomial constant

Note: $C_p = A(1) + A(2)\left(\frac{T}{1000}\right) + A(3)\left(\frac{T}{1000}\right)^2 + A(4)\left(\frac{T}{1000}\right)^3 + A(5)\left(\frac{1000}{T}\right)^2$ cal/mole

A(6) — enthalpy constant of integration

Note: $A(6) = \Delta H_f^\circ - \int_0^{298} C_p dT$ kcal/mole

CSA — entropy constant of integration cal/mole°K

Note: $s = \int_0^T C_p \frac{dT}{T} + CSA$ cal/mole°K

Card 42

FA(1)	Mass fraction composition of species in mixture α . Note: The species have to be input in the same order as used in the card set n.41 to n.44.

Card 43

FA(2)	Mass fraction composition of species in mixture β . Same note applies as for Card 42.

Card 44

FA(3)	Mass fraction composition of species in mixture γ . Same note applies as for Card 42.

The following cards contain the reaction mechanism and rate coefficients. They are read only if IKINE Card (38) is set nonzero.

Card 45.n

	column	
IZD(1)	1-4	species A
	7	+ sign
IZD(2)	8-11	species B
	14	+ sign
	15-20	blank or species M
	21	= sign
IZD(3)	22-25	species C
	28	+ sign (if needed)
IZD(4)	29-32	species D
	35	+ sign (if needed)
IZD(5)	36-39	species E
IRR	49,50	Reaction types (1 to 16)
IRT	51	Rate coefficient type (1 to 8)
RC(1)	52-59	Pre-exponential factor, A (cm-molecule-sec units)
RC(2)	60-63	Temperature exponent, N
RC(3)	64-72	Activation energy, E_A (cal/mole)

Note: The reaction rate $k = AT^{-N}\exp(-\frac{E_A}{RT})$. The equilibrium constant, K_p is determined from $\ell nK_p = -\Delta G/RT$

The reaction types are,

(1)		A + B	$\rightleftarrows$	C + D	
(2)		A + B + M	$\rightleftarrows$	C + M	
(3)		A + B	$\rightleftarrows$	C + D + E	
(4)		A + B	$\rightleftarrows$	C	
(5)		A + M	$\rightleftarrows$	C + D + M	
(6)	$(\alpha + \beta)$	A + B	$\rightarrow$	C + D	includes effect of turbulent fluctuations
(7)	$(\alpha + \gamma)$	A + B	$\rightarrow$	C + D	includes effect of turbulent fluctuations
(8)	$(\beta + \gamma)$	A + B	$\rightarrow$	C + D	includes effect of turbulent fluctuations
(9)	$(\alpha + \beta)$	A + B	$\rightarrow$	C	includes effect of turbulent fluctuations

The rate coefficient types are,

(1)	$k_f = A$
(2)	$k_f = AT^{-1}$
(3)	$k_f = AT^{-2}$
(4)	$k_f = AT^{-1/2}$
(5)	$k_f = A \exp(B/RT)$
(6)	$k_f = AT^{-1}\exp(B/RT)$
(7)	$k_f = AT^{-3/2}$
(8)	$k_f = AT^{-N}\exp(B/RT)$

APPENDIX D

Construction of the "Typical Eddy" Model

The procedure for the construction of the complete "typical eddy" model is illustrated below. For simplicity, only the species pdf is considered.

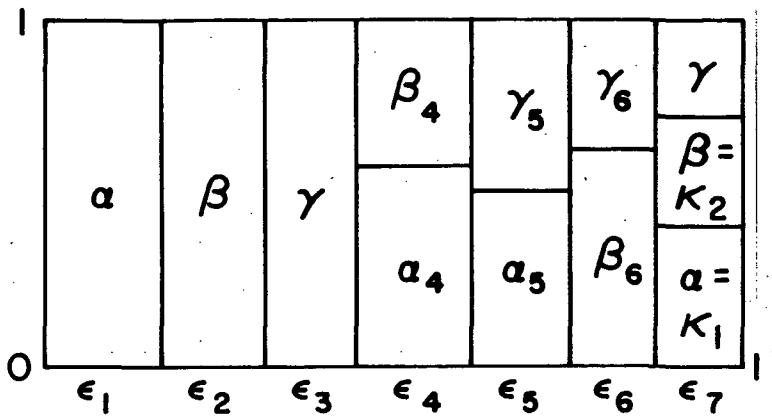

The model has eight parameters - ε_1 through ε_6, κ_1 and κ_2 which have to be calculated by matching the model moments to the moments obtained from the second-order closure calculation. The following nonlinear equations have to be solved.

$$\varepsilon_1 \cdot 1 + \alpha_4 \cdot \varepsilon_4 + \alpha_5 \varepsilon_5 + \kappa_1 \varepsilon_7 = \bar{\alpha}$$

$$\varepsilon_2 \cdot 1 + \beta_4 \varepsilon_4 + \beta_6 \cdot \varepsilon_6 + \kappa_2 \varepsilon_7 = \bar{\beta}$$

$$\varepsilon_1(1-\bar{\alpha})(-\bar{\beta}) + \varepsilon_2(-\bar{\alpha})(1-\bar{\beta}) + \varepsilon_3\bar{\alpha}\bar{\beta} + \varepsilon_4(\alpha_4-\bar{\alpha})(\beta_4-\bar{\beta}) + \varepsilon_5(\alpha_5-\bar{\alpha})(-\bar{\beta}) + \varepsilon_6(-\bar{\alpha})(\beta_6-\bar{\beta}) + \varepsilon_7(\kappa_1-\bar{\alpha})(\kappa_2-\bar{\beta}) = \overline{\alpha'\beta'}$$

$$\sum_{1-7} \varepsilon_i(\alpha_i-\bar{\alpha})(\gamma_i-\bar{\gamma}) = \overline{\alpha'\gamma'}$$

$$\sum_{1-7} \varepsilon_i(\beta_i-\bar{\beta})(\gamma_i-\bar{\gamma}) = \overline{\beta'\gamma'}$$

$$\varepsilon_1(1-\bar{\alpha})(\rho_1-\bar{\rho}) + \varepsilon_2(-\bar{\alpha})(\rho_2-\bar{\rho}) + \varepsilon_3(-\bar{\alpha})(\rho_3-\bar{\rho}) + \varepsilon_4(\alpha_4-\bar{\alpha})(\rho_4-\bar{\rho}) + \varepsilon_5(\alpha_5-\bar{\alpha})(\rho_5-\bar{\rho}) + \varepsilon_6(-\bar{\alpha})(\rho_6-\bar{\rho}) + \varepsilon_7(\kappa_1-\bar{\alpha})(\rho_7-\bar{\rho}) = \overline{\alpha'\rho'}$$

$$\sum_{1-7} \varepsilon_i(\beta_i-\bar{\beta})(\rho_i-\bar{\rho}) = \overline{\beta'\rho'}$$

$$\sum_{1-7} \varepsilon_i(\rho_i-\bar{\rho})^2 = \overline{\rho'\rho'}$$

These equations have to be solved numerically.

The construction of the simplified "typical eddy" model neglects the density correlations, and therefore, the species pdf can only have a total of five independent parameters. It is, therefore, necessary to make the following additional assumptions.

$$\kappa_1 = \bar{\alpha}$$

$$\kappa_2 = \bar{\beta}$$

$$\varepsilon_7 = \left(1 - \left|\frac{\overline{\alpha'\beta'}}{\bar{\alpha}\bar{\beta}}\right|\right)\left(1 - \left|\frac{\overline{\alpha'\gamma'}}{\bar{\alpha}\bar{\gamma}}\right|\right)\left(1 - \left|\frac{\overline{\beta'\gamma'}}{\bar{\beta}\bar{\gamma}}\right|\right)$$

The expression for ε_7 is selected to satisfy the reaction end limit. When the reaction is complete, $\overline{\alpha'\beta'}/\bar{\alpha}\bar{\beta} = -1$, and there should be no regions where the reactants α and β coexist. Thus, $\varepsilon_7 \equiv 0$, and also ε_4 goes to zero. The system of equations for ε_1 through ε_5 now becomes a set of linear algebraic equations and can be solved in closed form. The solutions are:

$$\varepsilon_1 = \bar{\alpha}(1-\varepsilon_7) - \alpha_4\varepsilon_4 - \alpha_5\varepsilon_5$$

$$\varepsilon_2 = \bar{\beta}(1-\varepsilon_7) - \beta_4\varepsilon_4 - \beta_6\varepsilon_6$$

$$\varepsilon_3 = \bar{\gamma}(1-\varepsilon_7) - \gamma_5\varepsilon_5 - \gamma_6\varepsilon_6$$

$$\varepsilon_4 = (\overline{\alpha'\beta'} + (1-\varepsilon_7)\bar{\alpha}\bar{\beta})/\alpha_4\beta_4$$

$$\varepsilon_5 = (\overline{\alpha'\gamma'} + (1-\varepsilon_7)\bar{\alpha}\bar{\gamma}/\alpha_5\gamma_5$$

$$\varepsilon_6 = (\overline{\beta'\gamma'} + (1-\varepsilon_7)\bar{\beta}\bar{\gamma})/\beta_6\gamma_6$$

The solutions of both the complete model and the simplified model involve ε_4, ε_5 and ε_6 as parameters. In previous computations we have assumed these as either all equal to 1/2 or equal to their mean proportion in the flow (e.g., $\varepsilon_4 = \bar{\alpha}/\bar{\alpha}+\bar{\beta}$, $\beta_6 = \bar{\beta}/\bar{\beta}+\bar{\gamma}$, etc.). The results of these two choices are about the same, and lead to occasional problems with the appearance of negative probabilities for the strengths of the delta functions. A solution to this problem has been developed recently, but is still undergoing testing. The procedure involves the determination of the range of values of ε_4 etc. for which valid pdf structures can be constructed and then selecting the proportions in the middle cells corresponding to the midrange value of a selected third moment. This procedure is successful in the construction of a two-species complete "typical eddy" that is always physically realistic over the entire range of statistically valid moments. It has to be tested now for the three-species model.